

Chaos Extension Radial Basis Function Neural Network Based on Fault Diagnosis Method for Solar Photovoltaic System Integrated in Inverters of the Three-Phase into the Electrical Grid of Congo-Brazzaville

Rostand Martialy Davy LOEMBE SOUAMY ^{#1,2,3,4,5,6} *, Johan Ange Abena ^{#2}, Christian Tathy ^{#3},
Guo-Ping Jiang ^{#4}, HongHuaWang ^{#5}, Xu Bao Wen ^{#6}

[#] *Laboratory of Electrical and Electronic Engineering (LGEE), National Higher Polytechnic School, Marien Ngouabi University, BP: 69, Brazzaville, Republic of the Congo¹*

[#] *Laboratory of Nanomaterials and Nanotechnologies, National Institute for Research in Exact and Natural Sciences (IRSEN) P.O. Box 2400, Brazzaville, Republic of Congo²*

[#] *Mechanical, Energy and Engineering Laboratory, Higher National Polytechnic, Marien Ngouabi. Univeristy Brazzaville, Republic of Congo. Department of Exact Sciences, Higher Teacher's Training School, Marien Ngouabi. Univeristy Brazzaville, Republic of Congo³*

[#] *School of Automation and Artificial Intelligence, Nanjing University of Posts and Telecommunications, Nanjing 210023, China⁴*

[#] *Laboratory of Control Theory and Control Engineering, Hohai University, College of Energy and Electrical Engineering, Nanjing 211100, China⁵*

[#] *Jiangsu Province Key Laboratory for Novel Technology, Department of Computers and Technology, Nanjing University, 210093, China⁶*

Email1: loembesouamy@gmail.com Email2: johan_abena@yahoo.fr Email1: Christian.tathy@umng.cg

* Corresponding Author: loembesouamy@gmail.com

Abstract— This paper investigates the chaos extension radial basis function neural network of Maximum Power Point Tracking (MPPT) algorithms based on fault diagnosis method in single-stage three-phase photovoltaic (PV) systems connected to the grid of Congo-Brazzaville and compares the attributes of various conventional, significance and in this study, a novel approach was developed to improve accuracy of intelligent controller system which is radial basis function neural network. However, once a fault occurs, in order to remedy the defect of unavailable fault diagnosis at any irradiance and temperature in this system chaos synchronization based intelligent fault diagnosis for photovoltaic systems proposed by others researchers. This paper describes a chaotic extension fault method combined and with error radial function to overcome this problem. The designed control functions ensure stable controlled and synchronized states for simulation and comparison, measured current irradiance and temperature, and used the Maximum Power Point Tracking (MPPT) algorithms for chaotic extraction of eigenvalue.

In the current research, the advanced of control was completed, a new strategy is being developed, so this structure is relatively complex because of their nonlinearity, the proposed of method which is MPPT, and the conversion efficiency is difficult improved due to increase in transformation series, three-layer artificial network for fault diagnosis and provided more accurate diagnostic response than on layer–fault diagnosis algorithms, axis neural network performance and techniques, and others Maximum Power Point Tracking (MPPT) algorithms in normal and partial shading conditions. The range of extension field was determined by neural network numerical simulations are implemented for illustration and verification of the effectiveness of radial basis function neural network control technique to the electrical grid of Republic of Congo and their influences on the dynamic performance of the system and their impact in reducing the harmonic rate for better injection into the grid, compared the diagnostic rates with the results indicate a significant increase in accuracy by others. A model of three single-phase PV grid-connected system is built, and simulation results show the MPPT algorithm has excellent dynamic and static performances, which verifies fault diagnosis method is effective for MPPT in the single-stage and three single-phase PV grid-connected system. Finally, the voltage eigenvalue obtained from current temperature and irradiance was used for the fault diagnosis

Keywords—: Photovoltaic array, Maximum Power Point Tracking, Radial Basis Function Neural Network, Partial Shading Conditions Chua’s System, State Observer Fault Diagnosis Method.

I. INTRODUCTION

This paper presents the background and the motivation of the chaos extension radial basis function neural network of Maximum Power Point Tracking (MPPT) algorithms continuing with a short overview of grid – connected PV system. Furthermore, in details the aims of the project, continuing with a list of the main contributions and finishing with the outline of the proposed method. This study focused on solar photovoltaic fault diagnosis. Photovoltaic (PV) energy generation provides several advantages such as harmless to the environment and renewable.

At present, the solar photovoltaic system has been used in many fields, current research focuses are the use of this technology, such as efficient storage, environmental issues, and subsequent maintenance. This continuously increasing energy consumption overloads the distributions grids as well as the power stations. Therefore, employing a neural network has a positive impact on managing power faults and maintaining normal operating conditions in [1]. Most of classical fault diagnosis technologies are based on intelligent control including neural network in [2]. Most of classical fault diagnosis technologies are based on intelligent control including neural network [3,4,5,6]. In 2011, Shimakage et al. discussed photovoltaic system fault diagnosis and used an algorithm and observation for diagnosis in [6]. In 2011, Syafaruddin et al. used three-layer artificial network for fault diagnosis. Also, this method was also time consuming in [7]. In 2012, Zhao et al, proposed a decision three based diagnostic method for photovoltaic system in [8].

Given the characteristics of photovoltaic (PV), such as their low efficiency and output dependency on environmental factors, it is crucial to monitor the maximum power point. While there are many strategies for maximum power point tracking, each with its advantages and disadvantages, some are better than others. For instance, previous research studies in (e.g. [4] ,[5]) have shown that the perturb and observe (P&O) algorithm has more strengths than others.

When it comes to photovoltaic systems, MPPT, there are two typical methods. By adjusting the angle of the module plane concerning the sun’s light, the first method involves mechanically measuring the amount of solar radiation that hits the PV module plates. This stops the system’s output power from declining as the intensity of the sun changes. The second method entails in the current research the DC-AC convert’s duty cycle in order to harness the full power of the PV modules in (e.g. [6], [7], [8], [9], [10], [11], [12], [13], [14]).

This approach beats the first approach because it provides effective power output without modifying the PV system's mechanically components.

This method was difficult to be implemented in [8]. In 2014, Hsiao et al used chaotic extension theory for diagnosis and the accuracy rate was high and how does to improve it? However, due to the limitation of extension theory, the diagnostic rate decreased greatly when the temperature and irradiance changed. This study aims to remedy the defects in the literature in [9]. In the literature in (e.g. [9], [10], [11], [12], [13], [14], [15], [16], [17], [18], [19], [20]), 10-series 2- parallel solar photovoltaic array was used as the model of fault diagnosis. Chaotic synchronization system was combined with externals for fault diagnosis.

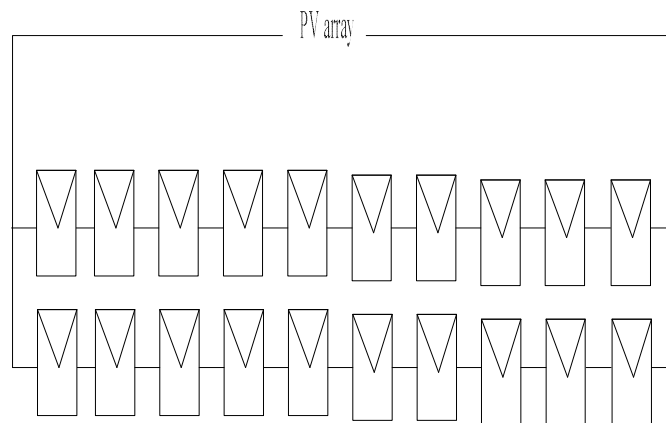


Fig. 1 10-series 2- parallel schematic diagram

The disadvantage with multi-stage system is that they have a relatively higher efficiency, large size and higher cost. The single stage has numerous advantages such as simple topology, low cost and high efficiency in (e.g. [5-6]). Nevertheless, the control strategy has to be designed in order to extract the maximum available power and to properly transfer it from the PV array to the grid simultaneously. In this case a most important consideration in the controller design is needed. The performance evaluation of MPPT schemes is imperative because of their sensitive to various dynamics in (e.g. [1], [2], [7], [8], [9], [10], [11], [12], [13], [14], [15], [16], [17], [18], [19], [20], [21], [22], [23-24]). This study presents a major innovation as it is the first to be applied to the specific case of the chaos extension radial basis function neural network of Maximum Power Point Tracking (MPPT) algorithms based on fault diagnosis method in single-stage three-phase photovoltaic (PV) systems connected to the grid of Congo-Brazzaville. Whereas MPPT control system schematic diagram shows as shown in Fig. 2

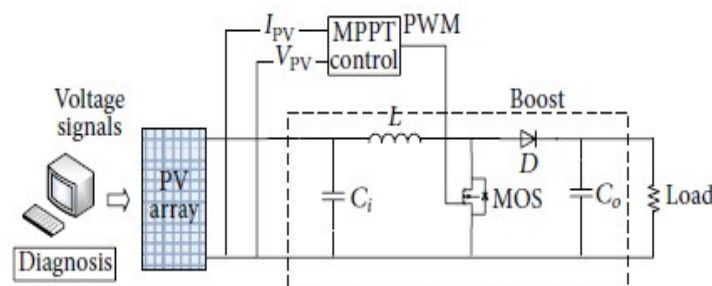


Fig. 2 MPPT control system schematic diagram

This paper is organized as follows. Section 2 presents a parallel schematic diagram, MPPT control a schematic diagram and Chua chaotic system. Section 3 presents system description and modeling of PV array system. Section 3.1 presents the dynamic parameters of the whole system and modeling of solar cell and PV array model. Section 3.2 presents photovoltaic characteristic and grid connected inverter model. Section 3.3 compares the dynamic parameters of Radial Basis Function Neural Networks algorithms and the dynamic parameters of Perturbation and observation (P&O) and Incremental Conductance (INC) algorithms. Section 3.4 presents the whole simulation results. Section 4.1 presents perturbation and observation ((P&O) techniques. Section 4.2 presents incremental conductance (INC) (techniques. Section 4.3 presents others MPPT schemes. Section 4.4 discusses the standard evaluating parameters partial shading conditions under different power and current. Section 5.1 presents a performance by comparing, one of them better of their big size, high cost, low efficiency and high reliability. Therefore, in three phase single-stage grid connected PV system must achieve MPPT. Therefore, in order to generate the MPPT stability under Irradiation and Temperature, a robust MPPT controller of radial basis function neural network has been proposed. Section 6.1 concludes this article.

II CHUA CHAOTIC SYSTEM

The design of the synchronization system of the Chua's chaotic system requires the following two methods, and the simulation is carried out with Matlab software to draw the synchronization error signal curve. The results indicate a significant increase in accuracy as follows as Drive-Response approach and State observer method system were analyzed. Untie: Chua's the equation of state for a chaotic system is as follows:

$$\begin{cases} \dot{x} = \alpha(y - x - f(x)) \\ \dot{y} = x - y + z \\ \dot{z} = -\beta y \end{cases} \quad (1)$$

There into, $\alpha > 0, \beta > 0, a < b < 0$, is a system parameter, $f(x) = bx + \frac{1}{2}(a-b)(|x+E| - |x-E|)$

Let the parameter values of the system be as follows as : $\alpha = 9.0, \beta = 14.87, a = -1.27, b = -0.68, E = 1$

A. Drive-Response

We Design process divide (1) into two subsystems:

$$\begin{cases} \dot{x} = \alpha(y - x - f(x)) & \text{Drive} \\ \begin{cases} \dot{y} = x - y + z \\ \dot{z} = -\beta y \end{cases} & \text{Response} \end{cases} \quad (2)$$

Copy the R system and get:

$$\begin{cases} \dot{y} = x - \hat{y} + \hat{z} \\ \dot{z} = -\beta \hat{y} \end{cases} \quad (3)$$

Therefore, the synchronization system is designed as follows as:

$$\begin{cases} \dot{x} = \alpha(y - x - f(x)) \\ \dot{y} = x - \hat{y} + \hat{z} \\ \dot{z} = -\beta\hat{y} \end{cases}$$

(4)

Then, the synchronization error signal is:

$$\begin{cases} \dot{e}_y(t) = -e_y + e_z \\ \dot{e}_z(t) = -\beta e_y \end{cases}$$

(5)

There into, $e_y = y - \hat{y}, e_z = z - \hat{z}$. Simulation process, take the simulation time range as $0 < t < 100$, and take the initial state $y_0 = [1, -0.5, -1, -10, 8]^T$ synchronization error signal.

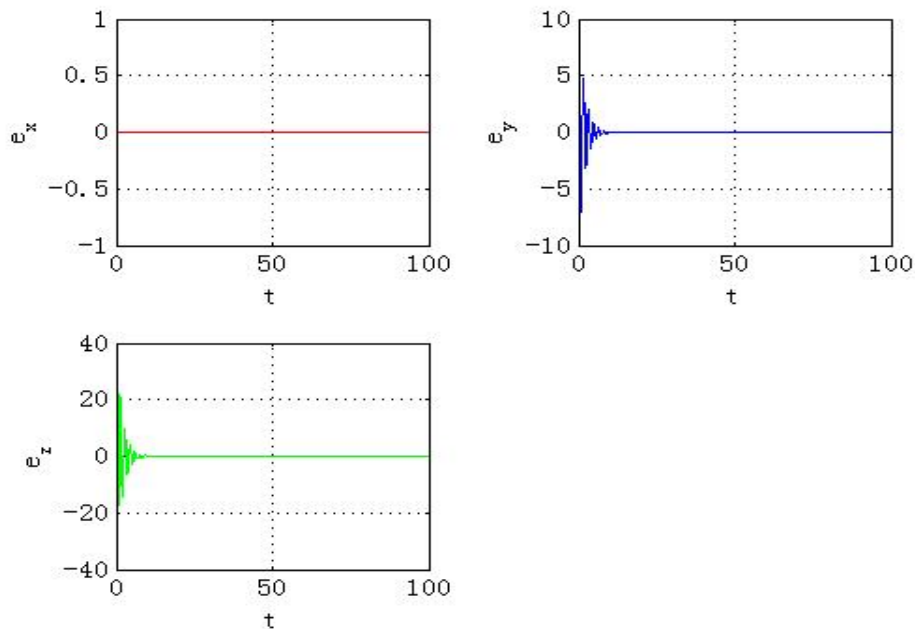


Fig. 3 Synchronization error signal line graph using colors which contrast a chaotic response

Whereas synchronization error signal shows the results indicate a significant increase in accuracy as shown in Fig. 3

B. State Observer Method

We designed Chua's equations of states of a circuit can be rewritten as:

$$\begin{cases} \dot{x} = Ax + BF(x) + C \\ Y = Kx + F(x) \end{cases}$$

(6)

There into,

$$A = \begin{bmatrix} -\alpha & \alpha & 0 \\ 1 & -1 & 1 \\ 0 & -\beta & 0 \end{bmatrix}, \quad B = \begin{bmatrix} -\alpha \\ 0 \\ 0 \end{bmatrix}, \quad C = \begin{bmatrix} 0 \\ 0 \\ 0 \end{bmatrix}, \quad F(x) = [f(x_1) \quad 0 \quad 0]$$

$$f(x_1) = bx_1 + \frac{1}{2}(a-b)(|x_1 + E| - |x_1 - E|),$$

$$Y = Kx + F(x).$$

For the output of the system, thee into K is a constant to be determined available by $(A - BK)$. The eigenvalue real part is negative. The equation of state for constructing a synchronous system using the method of state observer is as follows:

$$\begin{cases} \dot{\hat{x}} = A\hat{x} + BF(\hat{x}) + C + B(Y - \hat{Y}) \\ \hat{Y} = K\hat{x} + F(\hat{x}) \end{cases}$$

(7)

Then, the synchronization error signal is as follows as:

$$\dot{e} = (A - BK)e$$

(8)

To determine K consider $(A - BK)$, the eigenvalue of the matrix as follows as : $\lambda_1 = -29, \lambda_2 = -1 + i, \lambda_3 = -1 - i$. Then use the place instruction in Matlab to find K as : $K = [-2.3333 \quad -2.6811 \quad -2.8999]$. Take the simulation time range as $0 < t < 100$, take the initial state $y_0 = [1, -0.5, -1, -10, 8, 15]^T$. Synchronization error signal follows as:

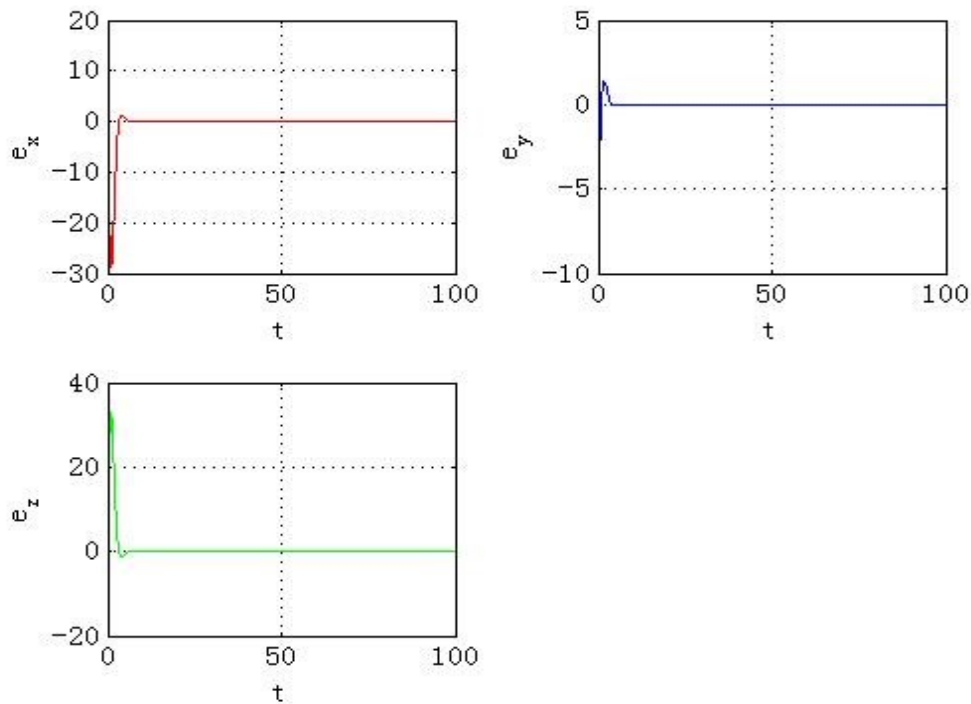


Fig. 4 Synchronization error signal line graph using state observer method

The results indicate also a significant increase in accuracy as shown in Fig. 4. As we mentioned, the purpose of fault diagnosis used in this paper is 10-series 2 parallel photovoltaic systems as shown in figure1 and MPPT, the system description, are shown in figure1. Also the specifications of PV cell are shown in Fig.5, Fig. 6 which are PV of characteristics MPPT results. The specifications of PV cell are shown Fig. 7, Fig. 8 and Fig. 9 given as $I_{sc}=5.3A$, $V_{oc}=100V$, $P_{max}=150W$, and according to our fault diagnosis used in our application systems shown as:

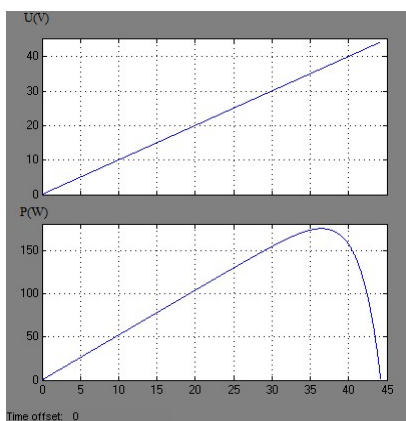


Fig. 5 Power and Voltage Versus

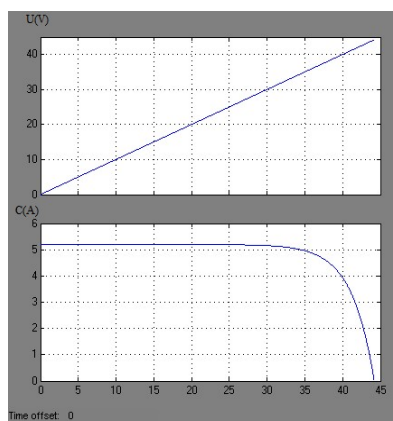


Fig. 6 Current and Voltage Versus

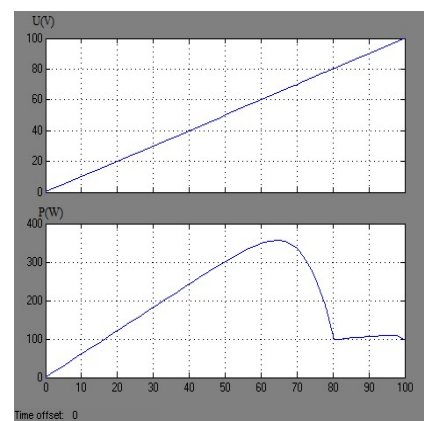


Fig. 7 Power Shading and Voltage Versus

The photovoltaic cell is set as short circuit to simulate nine fault states to be illustrated by simulations and the I-V and P-V characteristic curves at different irradiance and temperatures are satisfied functional

requirements and the shading satisfying performance requirements. This paper puts forward a fault detection mechanism, which is based on the theories of artificial neural network and probability change point analysis, to detect the system that fail to satisfy performance requirements.

III. SYSTEM DESCRIPTION AND MODELLING OF PHOTOVOLTAIC SYSTEM

A Solar Cell and PV array Model

In the present modeling, the focus is only on cells. Solar cells consist of a p-n junction. The simplest equivalent circuit of a solar cell is a current source in parallel with a diode. The diode determines the I-V characteristics of the cell. Whereas for this paper shows, the electrically equivalent circuit of a solar cell is shown in Fig.5, as shown in [2].

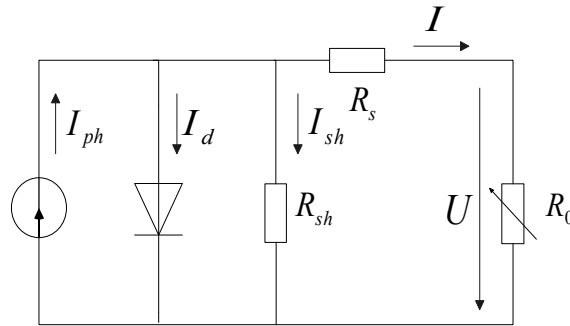


Fig. 8 Solar cell electrically equivalent

$$I = I_{ph} - I_d - I_{sh} = I_{ph} - I_{do} - \frac{V + IR_s}{R_{sh}} = I_{ph} - I_o \left\{ \exp \left[\frac{q(V + IR_s)}{AkT} \right] - 1 \right\} - \frac{V + IR_s}{R_{sh}} \quad (9)$$

$$I_o = I_{do} \left(\frac{T}{T_{ref}} \right)^3 \exp \left[\frac{qE_g}{nk} \left(\frac{1}{T_{ref}} - \frac{1}{T} \right) \right] \quad (10)$$

$$I_{ph} = \left\{ I_{sh} \left(\frac{S}{1000} \right) + C_T (T - T_{ref}) \right\} \quad (11)$$

$$I = I_{ph} - I_d = I_{ph} - I_o \left\{ \exp \left[\frac{q(V + IR_s)}{AkT} \right] - 1 \right\} \approx I_{ph} - I_o \left\{ \exp \left[\frac{qV}{AkT} \right] - 1 \right\} \quad (12)$$

When I=0 in formula (12), the open circuit voltage can be deduced as:

$$V_{OC} = \frac{nkT}{q} \ln \left(\frac{I_{ph}}{I_o} + 1 \right) \quad (13)$$

Here, I_{ph} is the photocurrent, I_o is the reverse saturation current, I_{do} is the average current through the diode, n is the diode factor, q is the electron charge ($q=1.6 \cdot 10^{-19}$), k is the Bolt man's constant ($k=1.38 \cdot 10^{-23}$ J/K), and T is the solar array panel temperature. R_s is the intrinsic series resistance of the solar cell; this value is normally very small, R_{sh} is the equivalent shunt resistance of the solar array, and its value is very large. I_{sc}

is photovoltaic battery short-circuit current; S is light intensity; C_T is the temperature coefficient; T is temperature of cell in Kelvin (K); T_{ref} is the reference temperature (298K); E_g is the characterization of the width of the forbidden band semiconductor constants(V). In general, the output current of a solar cell is expressed by: Physical models based on physical mechanisms and mathematical models based on external characteristic. The model parameter setting based on external characteristic is more realistic. The photovoltaic array is modeled as follows in (e.g.[3-4]): Under the conditions of any solar radiation intensity R ($w \cdot m^{-2}$) and ambient temperature T_a ($^{\circ}C$), the Photovoltaic array temperature T_c ($^{\circ}C$) is:

$$T_c = T_a + t_c \cdot R \quad (14)$$

In the formula , R is the light radiation of the Photovoltaic array and t_c ($w^{-1} \cdot m^2$). In the formula, R is the light radiation of the Photovoltaic array and t_c ($w^{-1} \cdot m^2$) is the temperature coefficient of the photovoltaic array. Under the reference, I_{sc} is the short –circuit current , V_{oc} is the open-circuit voltage, and I_m 、 V_m is the current and voltage at the maximum power point, then when the photovoltaic array voltage is V , its current , whereas I is the following equation represents the equivalence of short circuit current and temperature coefficient, fundamental to relativity, as follows as :

$$I = I_{sc} (1 - C_1 (e^{\frac{V}{C_2 V_{oc}}} - 1)) \quad (15)$$

Where C_1 represents the dynamic of parameter temperature coefficient, as follows as:

$$C_1 = (1 - I_m / I_{sc}) e^{-\frac{V_m}{C_2 V_{oc}}} \quad (16)$$

Where C_2 represents also the dynamic of parameter temperature coefficient, as follows as :

$$C_2 = (V_m / V_{oc} - 1) / \ln(1 - I_m / I_{sc}) \quad (17)$$

In the current research considering solar irradiation and temperature changes, as follows as:

$$I = I_{sc} (1 - C_1 (e^{\frac{V}{C_2 V_{oc}}} - 1)) + DI \quad (18)$$

Where DI are the average of current of solar and photovoltaic array, as follows as:

$$DI = \alpha \cdot R / R_{ref} \cdot DT + (R / R_{ref} - 1) \cdot I_{sc} \quad (19)$$

Where DV are the average of voltage of solar and photovoltaic array, as follows as:

$$DV = -\beta \cdot DT - R_s \cdot DI \quad (20)$$

Where DT are the average of temperature of solar and photovoltaic array, as follows as:

$$DT = T_c - T_{ref} \quad (21)$$

Where R_{ref} , T_{ref} are the reference values of solar radiation and photovoltaic array temperature, generally $1kW/m^2$, $25^{\circ}C$; where α represents : Under the reference sunshine, the temperature coefficient of

current change (Amps/ ° C); Where β represents : Under the reference sunshine, the temperature coefficient of voltage change (V/ ° C); Where R_s represents : The series resistance of the Photovoltaic array. An important parameter for evaluating the performance of photovoltaic cell is the fill factor(FF) which is in [5]:

$$FF = \frac{U_m I_m}{U_{oc} I_{sc}} \quad (22)$$

The molecule in formula (15) is P_m and the fill factor reflects the conversion efficiency of the photovoltaic array to a certain extent. The maximum conversion efficiency that a photovoltaic can obtain is in Ref [5]:

$$\eta_m = \frac{P_m}{P_{in}} \quad (23)$$

B Photovoltaic Characteristic and Grid Connected inverter

According to the characteristics of solar energy photovoltaic battery monomer equation according to of certain rules of series and parallel form photovoltaic array change different intensity of illumination and temperature, we applied as shown in Fig. 9 and as shown also in Fig. 10 of photovoltaic array nonlinear output characteristic curve is:

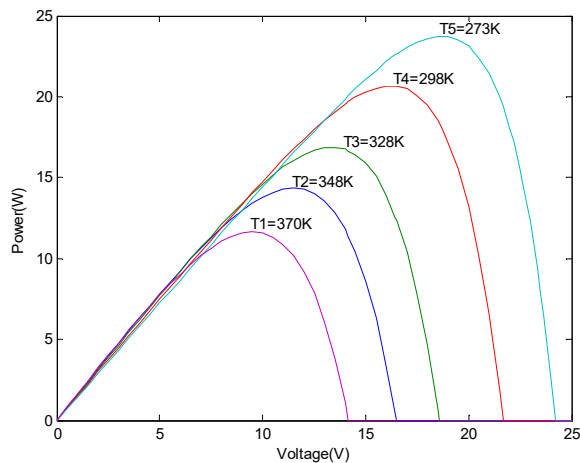


Fig. 9 PV cell characteristic curves under different-temperature (S=500W/m²) (T=273K)

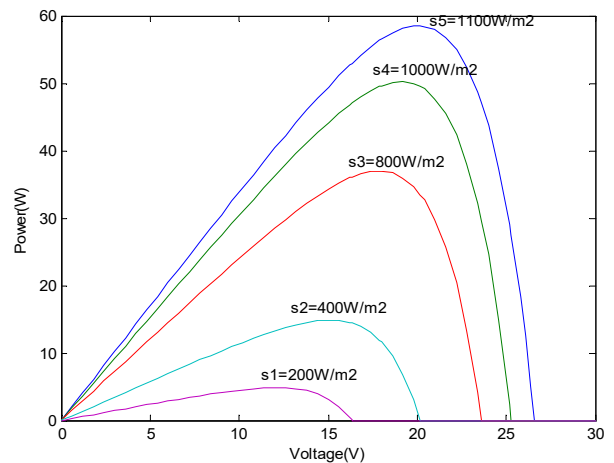


Fig. 10 PV cell characteristic curves under different- illuminations

A control strategy is being developed, the analysis of the PV cell characteristic under different –temperature and PV cell characteristic under different –illuminations of the data reveals significant trends, the experiment shows a strong result, as shown in Fig. 9 and Fig.10.

Whereas Topology shows a diagram of three-phase photovoltaic system connected to an inverter. As shown in Fig. 11:

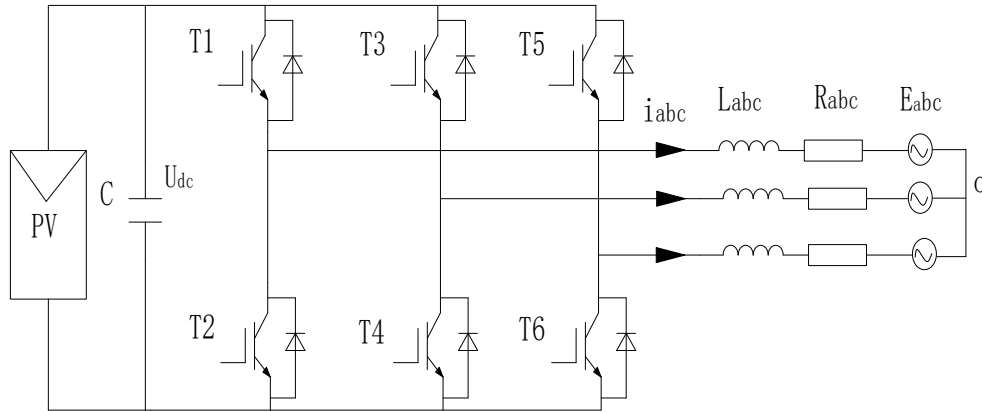


Fig. 11 Three phase photovoltaic grid –connected inverter model

PV represents the photovoltaic panel, C is the DC bus capacitor, T1 to T6 are the six IGBTs of the three inverter bridge in [6-7]. In the three- phase stationary coordinate system, according to Kirchoff's current and voltage laws, the current and voltage equations of the grid –connected inverter can be obtained as shown in [7]:

$$C_1 \frac{du_{dc}}{dt} = i_{pv} - \sum_k i_k s_k \quad (24)$$

$$L \frac{di_k}{dt} + Ri_k = u_{kn} - u_{sk} - u_{on} \quad (25)$$

$$u_{kn} = u_{dc} \cdot s_k$$

$$(26)$$

$$u_{kn} = u_{ko} + u_{on}$$

$$(27)$$

$$\sum_k i_k = \sum_k u_{sk} = 0 \quad (28)$$

Because the load of the photovoltaic inverter is symmetrical, the neutral point is 0. According to equations (25) (29) it can be obtained:

$$u_{on} = \frac{u_{dc}}{3} \cdot \sum_k s_k \quad (29)$$

$$\sum_k u_{ko} = \sum_k u_{kn} - 3u_{on} = 0$$

(30)

Where $k = a, b, c$, represents the switching state of an inverter bridge: When $s_k = 1$ indicates the upper arm of the PV inverter is on and the lower arm is off, and $s_k = 0$ indicates the upper arm is off and the lower arm is on. The inverter model in the three-phase stationary coordinate system is straightforward, but time-varying grid components complicate controller design. To simplify, this paper transforms the model from the three-phase stationary system to the synchronous rotating (d-q) system with the grid frequency. This conversion changes AC components to DC, easing control design. First, Clarke transformation converts the three-phase system to a two-phase stationary system, aligned with phase A of the grid in Ref [8]. Whereas Fig 12 shows the mathematical model of the photovoltaic inverter under synchronous coordinates, as shown in Fig. 12.

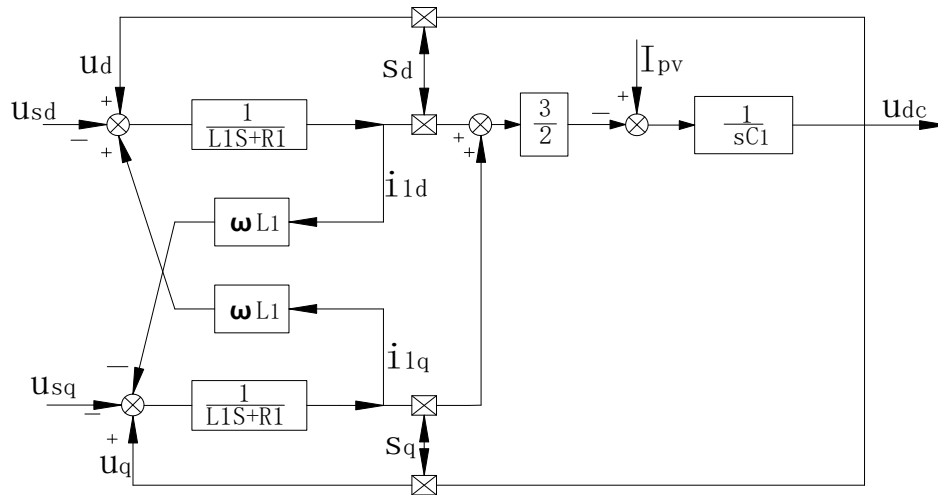


Fig. 12 Mathematical model of the photovoltaic inverter under synchronous coordinates

When the grid voltage is constant and inverter losses are neglected, the DC voltage of the grid-connected inverter is proportional to the d-axis component of the output current, and the active power p is also proportional to this current. Whereas the Fig.13 shows the DC voltage can be controlled by regulating the active power as shown in [9].

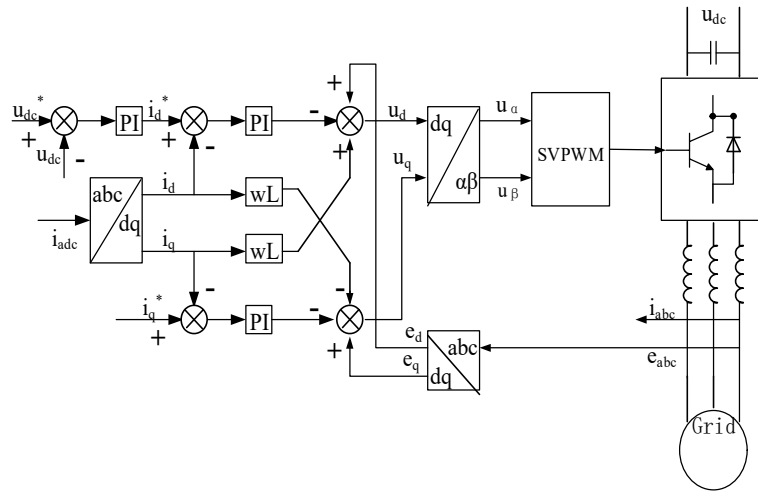


Fig. 13 Grid- connected inverter control block diagram based on grid voltage orientation

Whereas the Fig. 13 shows that the grid-connected inverter control system has an outer DC voltage loop and an inner loop for active and reactive currents. The DC voltage loop stabilizes or adjusts the DC side voltage. Due to the single-stage topology, the system often faces energy accumulation and DC voltage variations, which can lead to system collapse. DC voltage feedback can be achieved without static control using a PI controller. The design of the voltage loop primarily aims to enhance the power supply's ability to withstand interference with the load and is designed according to a type II system. To reduce overshoot, a filter link can be added to the reference voltage, or a ramp setting can be used to make the reference voltage change gradually. Assuming that the three-phase currents are symmetrical, the instantaneous power on the three-phase AC inductor is zero. We designed the data to determine the correlation as follows as:

$$C_1 \frac{du_{dc}}{dt} \cdot u_{dc} = u_{dc} i_{pv} - \frac{3}{2} e_d i_d \quad (31)$$

It is further transformed to:

$$C_1 \frac{du_{dc}}{dt} = i_{pv} - \frac{3e_d}{2u_{dc}} i_d \quad (32)$$

Since the values of e_d and u_{dc} do not change much $-3e_d / 2u_{dc}$, it can be represented by the constant K. Without considering the DC side disturbance, the transfer functions of active current and Dc voltage are expressed as follows as:

$$\frac{U_{dc}(s)}{I_d(s)} = \frac{K}{s C_1} \quad (33)$$

Let the PI regulator control equation be as follows as:

$$i_q^* = \left(K_p + \frac{K_i}{s} \right) (u_{dc}^* - u_{dc}) = K_p \left(\frac{\tau s + 1}{\tau s} \right) (u_{dc}^* - u_{dc}) \quad (34)$$

Knowing the current closed-loop transfer function, $w(s) = 1 / (3T_s s + 1)$ and considering the DC voltage sampling delay (e^{-T_s}), it can be approximated as $1 / (Ts + 1) = 1 / (4T_s + 1)$. Combine equations (34) and (35) to get the voltage open-loop transfer function, as follows :

$$\omega_o(s) = \frac{K_p K (\tau s + 1)}{C_1 \tau s^2 (Ts + 1)} \quad (35)$$

According to a typical type II system design there are:

$$\frac{K_p K}{C_1 \tau} = \frac{h + 1}{2\tau^2} \quad (36)$$

Taking the intermediate bandwidth, $h = \frac{\tau}{4T_s} = 5$, we get as follows as :

$$K_p = \frac{3C_1}{20KT_s} \quad (37)$$

$$K_i = \frac{K_p}{20T_s} \quad (38)$$

Design of the current loop PI, the sampling period of the current loop is the PWM switching period, T_s the data acquisition $e^{-T_s s}$ and $e^{-0.5T_s s}$ control delays are respectively, the delay link can be equivalent to $1 / (1.5T_s s + 1)$. The d and q-axis current control is symmetrical control, so taking the d-axis as an example, S-domain model of the PI controller is as follows as:

$$k_p + \frac{k_i}{s} = \frac{k_p (\tau_i s + 1)}{\tau_i s} \quad (39)$$

According to the typical $\tau_i = L/R$, the Figure 5 as shown of the PI controller is as follows :

$$W_o(s) = \frac{k_p}{R\tau_i s (1.5T_s s + 1)} \quad (40)$$

Then the PI controller parameters can be obtained as follows as:

$$k_p = \frac{R\tau_i}{3T_s} = \frac{L}{3T_s} \quad (41)$$

$$k_i = \frac{k_p}{\tau_i} \quad (42)$$

Where k_p and k_i are the proportion coefficient and integral coefficient, respectively. In this paper, we connected the photovoltaic system-inverter to the electricity grid of the Republic of Congo. The schematic representation of the electricity transmission network, shown in a single-line diagram (see Fig. 14), provides a detailed overview of the elements of this complex network. This representation is crucial for understanding the layout and operation of the components that ensure electricity distribution across the country. Firstly, the network consists of five power generation plants: The Congo Electric Power Plant (CEC) at node (1) located in the Pointe-Noire department, the Imboulou Power Plant at node (34) situated in the Pool department, the Djeno Power Plant at node (6) in the Pointe-Noire department, the Moukoulou Power Plant at node (19) in the Bouenza department, and finally, the Djoué Power Plant at node (23) in the Pool department, which is currently out of service. These plants play a crucial role in generating the energy necessary to supply the country. They are strategically located at various points across the Congolese territory to meet energy needs in a balanced manner. The geographical distribution of these plants aims to optimize production and minimize line losses. Regarding consumption, the network includes 22 loads, representing the various locations where electricity is used. These loads are primarily localities situated across different departments throughout the network. Effective management of these loads is essential to ensure a stable and reliable supply to end users. The network also features 24 transmission lines, which transport the electricity produced by the power plants to the loads. These lines often cover long distances, requiring rigorous planning and careful management to maintain distribution reliability. The transmission line infrastructure must be meticulously designed to minimize interruptions and ensure continuous delivery of electricity. Finally, the network comprises 34 nodes, which are convergence points for the transmission lines. These nodes play a strategic role in the network by allowing the redistribution of electricity in various directions. Through these nodes, the network can be organized in a meshed manner, significantly improving supply security. In the event of a failure or malfunction in part of the network, the nodes enable the redirection of electricity through alternative routes, thereby ensuring service continuity.

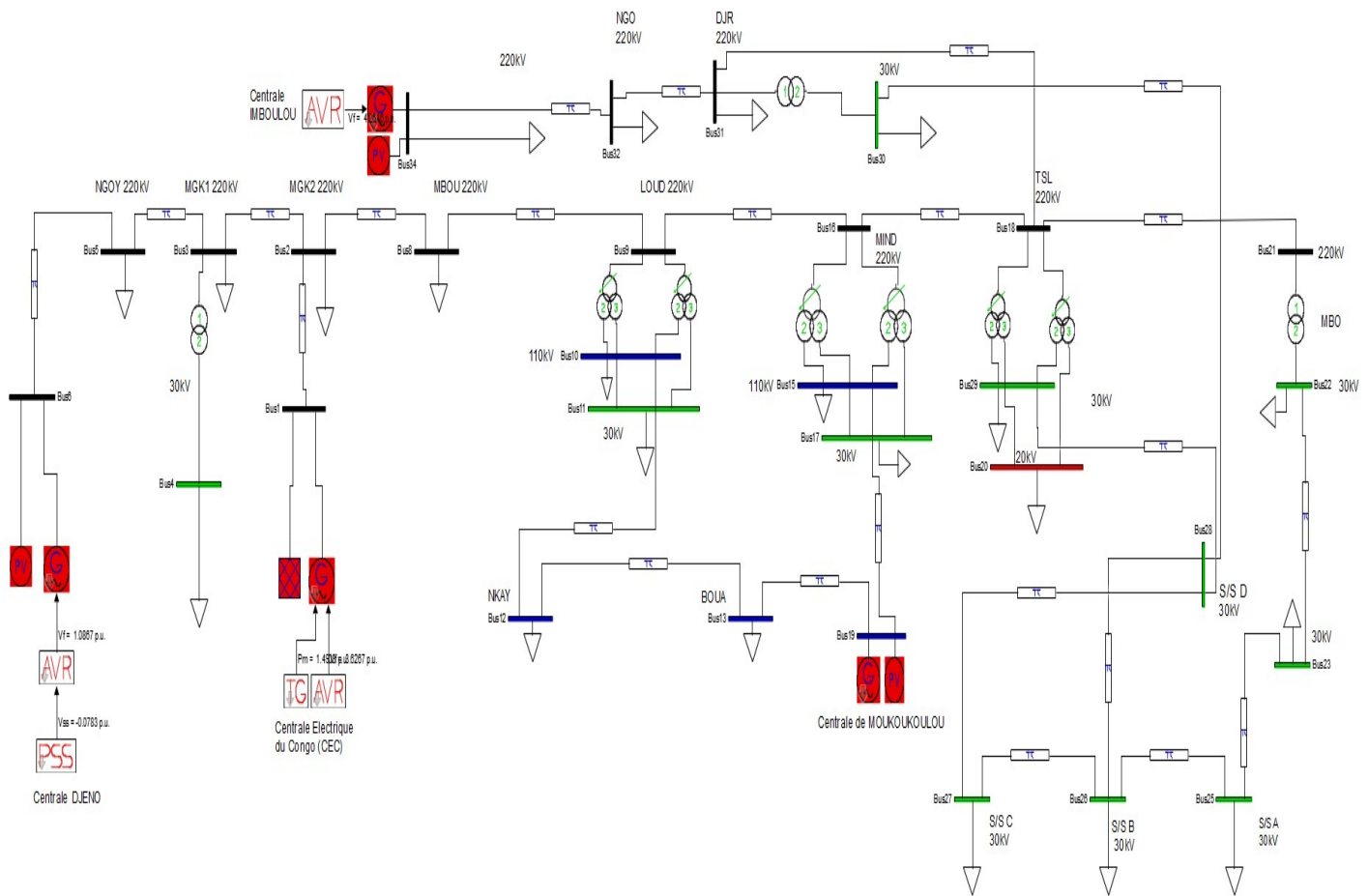


Fig.14 Power transmission network of the Republic of Congo

The geographic and schematic representation of the electricity transmission network of the Republic of Congo offers a detailed and precise view of the entire system. It clearly visualizes the arrangement of power plants, loads, transmission lines, and nodes. Whereas shows this comprehensive view is essential for effective network management, facilitating its maintenance and future improvements as shown in Fig. 14.

C Principle of MPPT control based on the Radial Basis Function Neural Network Algorithm

The RBFNN consists of three layers which include an input layer, a hidden layer, and an output layer arranged in a feedforward structure as can be seen in Fig. 15.

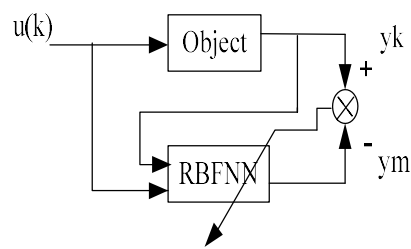


Fig..15 Controller of Radial Basis Function Neural Network

In the current research we developed a novel approach to improve accuracy Maximum for Power Point tracking (MPPT), is crucial in photovoltaic (PV) systems to ensure maximum efficiency by dynamically adjusting the operating point. Traditional MPPT methods(such as Perturb & Observe, Incremental Conductance) have limitations in dynamic performance and and adaptability under rapidly changing environmental conditions. Our approach to function approximation that is closely related to distance weighted regression and also to artificial neural network is learning with radial basis function. The typical mathematical structure for an RBFNN can be expressed in this approach, the learned hypothesis is a function of the form :

$$y(x) = \sum_{i=1}^n \omega_i \Phi(\|x - c_i\|) + b \tag{43}$$

The generated RBFNN automatically determines the number of required neurons on hidden layer through training, training starts from one neuron. It automatically increases neurons by checking the output error until the error sum of squares is less than the target error or the number of neurons achieves the maximal set value. Topology diagram of RBFNN system connected to an MPPT. As shown in Fig.16

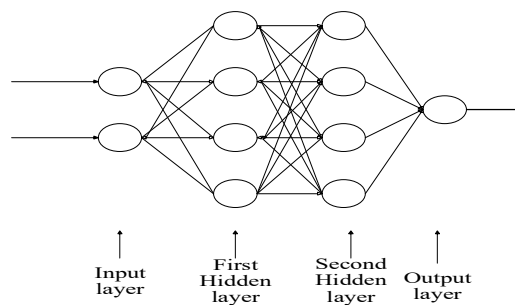


Fig.16 Photovoltaic array Radial Basis Function neural network structure

Whereas shows according to the general principle of the RBF network mapping, the proposed of method RBF network, for a PV array as shown in Fig.16. This comprises three layers: the input layer, the hidden layer and the output layer. The input layer consists of a three- dimensional vector X whose elements are radiation, ambient temperature and load voltage. The output layer has only one element, i.e. the load current, though in general it can be a vector of any dimension. The hidden layer is composed of M RBFs ϕ_j ($j = 1, L, , M$) that

are connected directly to all the elements in the input layer. For a data set consisting of N input vectors together which corresponding output currents, there are N such hidden units, each corresponding to one data point.

Thus we have:

$$X^n \begin{bmatrix} R_{ad}^n \\ T_a^n \\ V^n \end{bmatrix}, Y^n = I^n \quad (n = 1, 2, L, N)$$

(44)

The hidden unit can be expressed as a matrix as follows:

$$\Phi = \begin{bmatrix} \phi_1^1 & \phi_2^1 L & \phi_M^1 \\ \phi_1^2 & \phi_2^2 L & \phi_M^2 \\ M & M & M \\ \phi_1^N & \phi_2^N & \phi_M^N \end{bmatrix}$$

(45)

And the weight vector as follows:

$$W = \begin{bmatrix} \omega_1, k \\ \omega_2, k \\ M \\ \omega_M, k \end{bmatrix} (k = 1)$$

(46)

The function $\phi_j(X^n)$ takes the form of a nonlinear distribution. The one commonly used is the Gaussian function of the following as:

$$\phi_j(X^n) = \exp\left(\frac{\|X^n - C_j\|^2}{r^2}\right) \quad (47)$$

Where C_j ($j = 1, 2, L, M$), a vector having the same dimension as X , represents the center of the RBF ϕ_j and r is a scalar defining the width of an RBF, sometimes called spread constant(sc). Fig17 shows a typical Gaussian function response at $r = 1$ and $-5 < \|X^n - C_j\| < 5$.

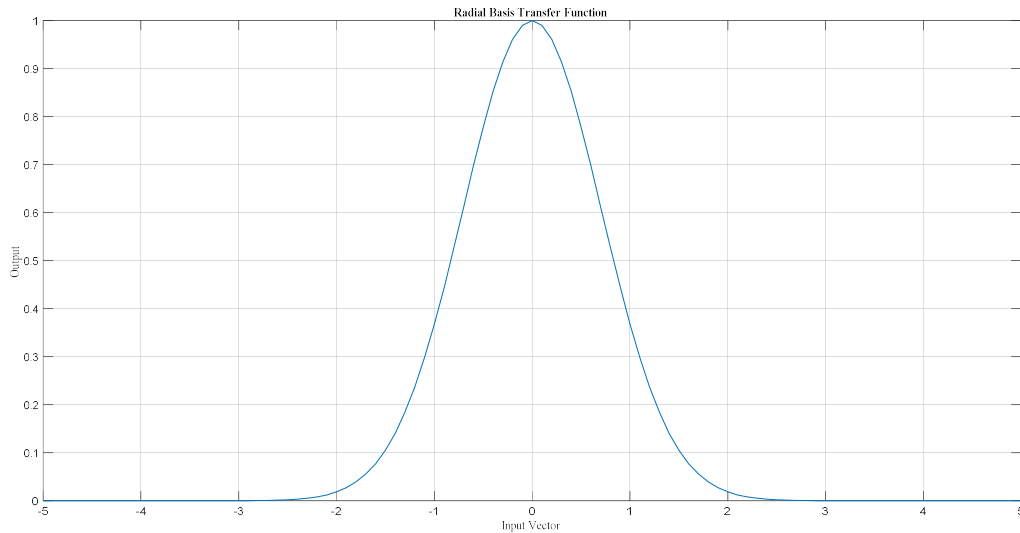


Fig..17 Typical radial basis function response at $r = 1$ and $-5 < \|X^n - C_j\| < 5$.

Each element of the output vector (in the Photovoltaic array application it is a scalar) Y^n is taken to be linearly weighted sum of M basis functions given as follows as :

$$y_k^n(X^n) = \sum_{j=1}^n \omega_{jk} \phi_j(X^n) + b_j \quad (48)$$

Where $y_k^n(X^n)$ is the k th element of $Y^n(X^n)$, ω_{jk} and b_j are the weighting factor and bias of the linear layer, respectively, b_j . Compensates for the difference between the average value over the dataset of the RBFs activation and the corresponding average value of the target outputs. In order to improve the goal optimization ability of the RBFNN and prevent getting trapped in local minima, a chaotic map is introduced. The chaotic map is used for parameter initialization or weight optimization common chaotic maps include:

-Logistic map as follows as:

$$x_{n+1} = \mu x_n (1 - x_n) \quad (49)$$

Where μ is a control parameter and $x_n \in (0,1)$.

-Tent map as follows:

$$x_{n+1} = \begin{cases} \frac{2x_n}{\lambda} & 0 \leq x_n \leq \frac{\lambda}{2} \\ \frac{2(1-x_n)}{\lambda} & \frac{\lambda}{2} \leq x_n \leq 1. \end{cases} \quad (50)$$

Where $\lambda \in (0,2)$. The chaotic sequence is used to initialize the weights, bias, and center parameter of the RBFNN. With the above described structure, the transformation from the input space to hidden layer is nonlinear, due to the use of Gaussian functions for RBFs. Whereas Table 1: shows the PV array parameters predicted by RBFNN on April 1-04-2025 in Congo-Brazzaville. Table 1: shows the PV array parameters

Time (h)	Instantaneous Irradiation (W/m ²)	Irradiation for one hour (Wh/m ²)	Temperature (°C)
7h 00	68	68	24

predicted by RBFNN on April 1-04-2025 in Congo-Brazzaville.

8h 00	155	155	25
9h 00	158	158	26
10h 00	204	204	28
11h 00	234	234	29
12h 00	245	245	30
13h 00	568	568	32
14h 00	396	396	34
15h 00	195	195	30
16h 00	271	271	29
17h 00	104	104	28,5

The hidden layer linked to the output layer, however, is linear. The main advantages of this configuration are that, it keeps the intelligence of modern control theory and the computation relatively enhanced. Training an RBF network involves determining an adequate number of RBFs and optimal values of the centers, weights and biases. The criterion is to minimize the sum of squared errors(SSE) defined as follows:

$$SSE = \frac{1}{2} \sum_n \sum_k \{t_k^n - y_k^n(X^n)\} \quad (51)$$

Where t_k^n (in this application $k = 1$) are the target values of the networks output when the network is presented with input vector X^n . Thus it is often only used to provide a set of starting values for an iterative process. One of the most commonly used schemes in self organizing approaches the orthogonal least-squares method which is used in this research to train the PV RBF network, in (e. g. [22], [23]). Values of weights are also determined at the same time. A straightforward procedure for doing this is to use the pseudo inverse method. In this case, the formal solution of the weights in matrix form is given by:

$$W^T = [\Phi^T \quad \Phi] \Phi^T T \quad (52)$$

The width parameters r_j of the RBFs may be calculated by many techniques. One heuristic approach is to choose all widths to be equal and to be given by about twice the average spacing between the basis function centers. Whereas Fig. 18 shows in the configuration of training data of network diagram, this ensures that the basis function overlap to some degree and hence give a relatively smooth representation of the distribution of training data of network diagram as shown in Fig. 18.

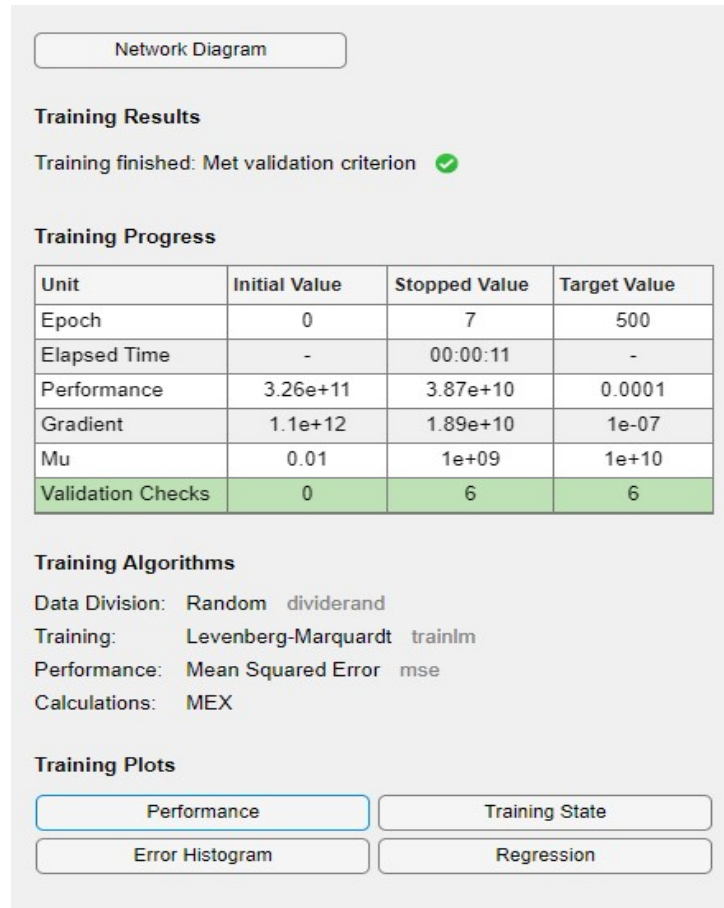


Fig.18 Training data of radial basis function neural network diagram

In order to improve the goal optimization ability of the RBFNN and prevent getting trapped in local minima, a chaotic map is introduced. The chaotic map is used for parameter initialization or weight optimization common chaotic.

Assumptions 1: The basis band of RBFNN is as $\sigma^u = (\sigma_1, L, \sigma_n)$, σ_j is a variance parameter of a simple pole j , the weighted matrix is $\omega^u = [\omega_1, L, \omega_j, L, \omega_m]^T$. In the extension theory, the matter–element is basic describing things which is the mathematical model applied to extension, defined as follows as in [12].

Whereas Fig. 19 shows an example of algorithm flowchart with adequate resolution of the schematic diagram as shown in Fig. 19, a new strategy is being developed on the diagnostics results indicate, as shown in Fig.20.

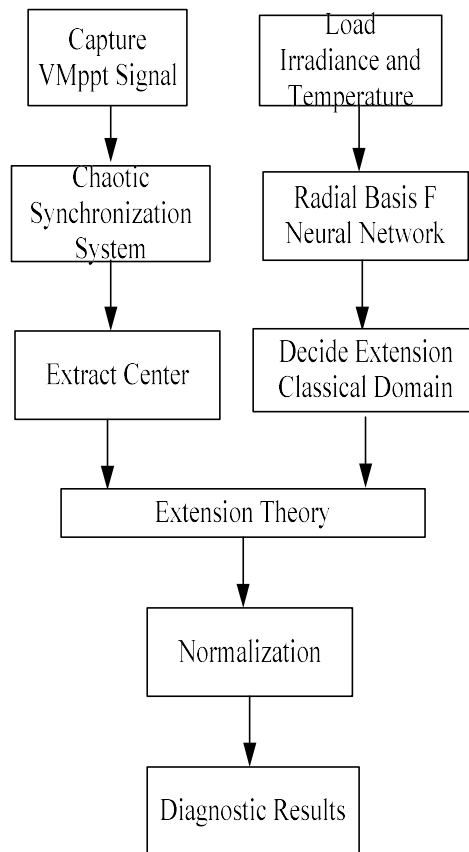


Fig. 19 System diagnosis process of chaotic extension neural network

The systems are imported into Radial basis neural network system to obtain the extension classical domain range of chaos center eigenvalue at current irradiance and temperature, and the recorded voltage is imported into the chaos synchronization. Whereas Fig. 20 shows an example of an acquisition data and control engineering with adequate resolution of the schematic diagram as shown in Fig. 20.

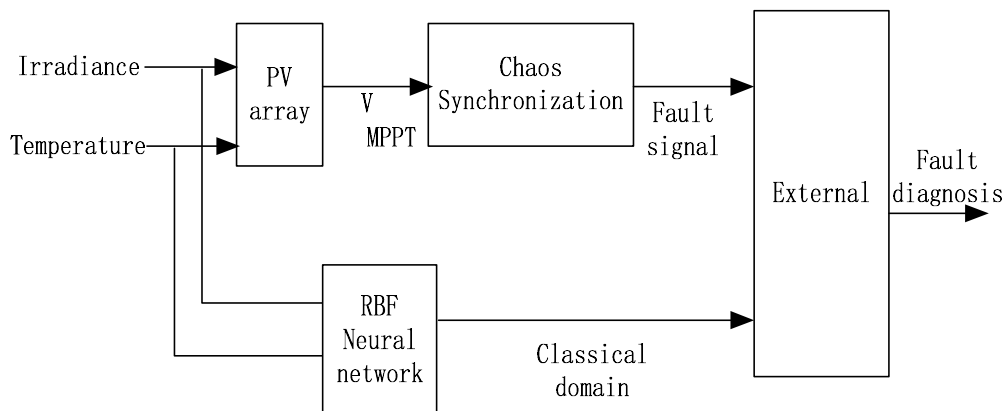


Fig.20. Schematic diagram of system diagnosis of chaotic extension neural network.

The neural network consists of multiple layers of neurons; the input end is called input layer and the output end is called output layer. The hidden layer is between the output layer and input layer Radial basis vector is $H = [h_1, \dots, h_m]^T$, h_j is the Gaussian basis function of node j , i.e., $h_j = \exp\left[-\frac{\|x - c_j\|^2}{2\sigma_j^2}\right]$

D. Performance of Radial Basis Function Neural Network

The proposed of method was completed increase in accuracy, then the training process involves updating the parameters of the network to minimize the error between the predicted output and the actual output. The error function can be represented as follows:

$$E(k) = \frac{1}{2} \sum_{k=1}^m (y(k) - y_m(k))^2 \quad (53)$$

To optimize the parameters gradient based methods or evolutionary algorithms enhanced by chaos optimization are employed. Fault diagnosis mechanism, the C-ERBFNN model can be trained on normal and faulty operating conditions of the PV systems partial shading or degradation. After training, the C-ERBFNN model can classify new input data into one of these fault categories based on the learned patterns. According to the gradient descent method, the output weighted vector, the node base width parameter and iterative algorithm of the node center vector, we have this following equations:

$$\omega_j(k) = \omega_j(k-1) + \eta \cdot (y(k) - y_m(k)) \cdot h_j + \alpha[\omega_j(k-1) - \omega_j(k-2)] \quad (54)$$

where η is study ratio $\in [0,1]$, α is the factor of momentum. The variation of variance parameters as follows:

$$\Delta\sigma_j = [(y(k) - y_m(k))\omega_j \cdot h_j] \cdot \left[-\frac{\|x - c_j\|^2}{2\sigma_j^2}\right] \quad (55)$$

Where $\sigma_j(k) = \sigma_j(k-1) + \eta \cdot \Delta\sigma_j + \alpha[\sigma_j(k-1) - \sigma_j(k-2)]$. In obtaining the voltage signal, the input to the single neuron RBF is the real power deviation signal and weight adjustment is done in using the error surface as C. The parameter C used to create the error surface. It follows that

$$\Delta C_{ji} = [y(k) - y_m(k)] \cdot \omega_j \cdot \frac{x - c_{ji}}{\sigma_j^2} \quad (56)$$

Where $\Delta C_{ji} = C_{ji}(k-1) + \eta \cdot C_{ji} + \alpha[C_{ji}(k-1) - C_{ji}(k-2)]$, also α is the factor of momentum, η is ratio $\in [0,1]$. Her-Term Yau as in [9], used a proposed method which is Back propagation, a multilayer feed forward network, in the basic back propagation training algorithm the weights are moved in the direction of the negative gradient.

Remark1:(e.g. [1], [2], [3], [4], [5], [6], [7], [8], [9], [12], [14], [19], [22], [23-24]), during training the weights and biases of the network are iteratively adjusted to minimize the network performance function. From Eqs. (57) and Eqs. (60), the RBF network can be viewed as approximating a desired function a function by superposition of non-orthogonal, bell shaped basis functions. The degree of accuracy of these RBF

networks can be controlled by three parameters of PV load. As an example The scope $\frac{\Delta P}{\Delta U}$ can be calculated using the PV module voltage and current based on P&O algorithm. The incremental conductance algorithm is derived by differentiating the PV module power with respect to voltage and setting the results equal to zero. For a direct control scheme which directly controls the converter switching without external control loops, the considered step is the change in converter duty ratio ΔD as shown in Equations (57,58,59,60).

$$\Delta D = N_1 \frac{\Delta P}{\Delta U} \quad (57)$$

$$\Delta P = P(k) - P(k-1) \quad (58)$$

$$\Delta U = U(k) - U(k-1) \quad (59)$$

$$\Delta D = D(k) - D(k-1) \quad (60)$$

And N_1 is the scaling factor tuned at the design stage to adjust the conventional step-size ΔD to compromise between tracking accuracy as in (e.g.[10],[18]) and its convergence speed.

E. Figures and Tables

This study purpose to remedy the defect of unavailable diagnosis at varying irradiance and temperature in the literature in [9], the RBF neural network is adopted. Fig. 20 is showing that the schematic diagram of system diagnosis at varying irradiation and temperature parameters. Whereas the figure shows an example of the I-V and P-V characteristic curves are different in different states luminous radiation power, irradiance is a measure of the power of luminous radiation received per unit area. In other words, it is the amount of light energy falling on a given surface per unit of time Fig. 21 and Fig. 22 as shown the evolution of luminous radiation power per unit area in (e.g. [12], [23]). Fig.23 as shown that is used for controlling the voltage of the converters to grid –connection. Fig.24 is showing that the MPPT of RBFNN method by comparing the training of data. The fault category is the short circuit in the solar panel of photovoltaic array, one normal state and fault state, as shown in the Fig. 26, the additional noise makes the kinematic trajectory of chaos system easier to be identified. Fig. 28 is showing that the system diagnostic of chaotic analysis neural network based on fault diagnosis on MPPT of RBFNN normal operation and fault operation power, current and voltage variation.

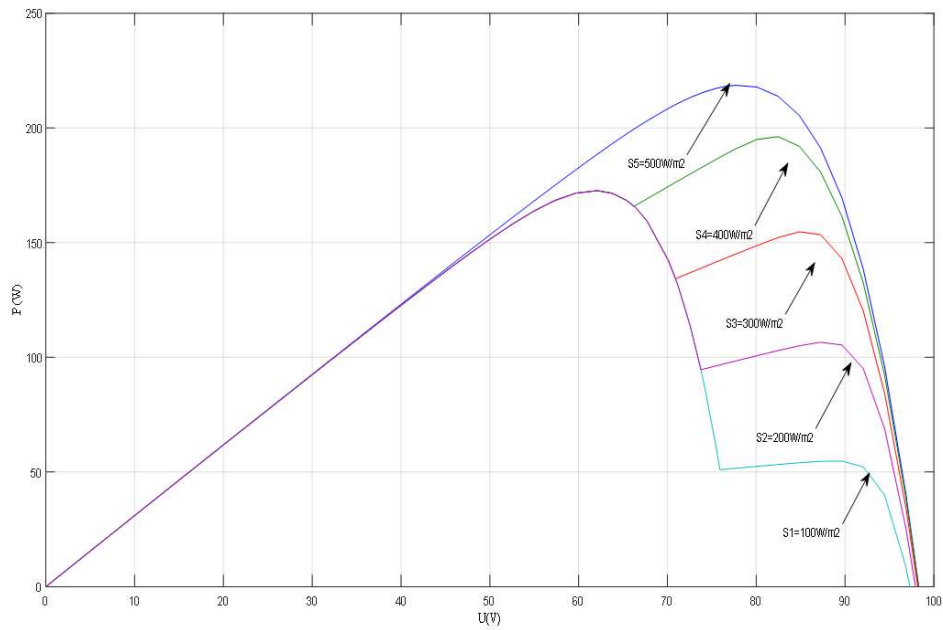


Fig. 21 Partial shading conditions under different luminous radiation power

It is observed from Fig.22. that the luminous radiation power is approximately 220 W for an irradiance of 500 W/m^2 , which corresponds to a surface area of 0.4 m^2 .

It is also noted that this radiation power decreases proportionally with the irradiance. Current variation with irradiated area, an increase in irradiance results in an increase in current for all voltage values, illustrated as shown in Fig. 23 Below.

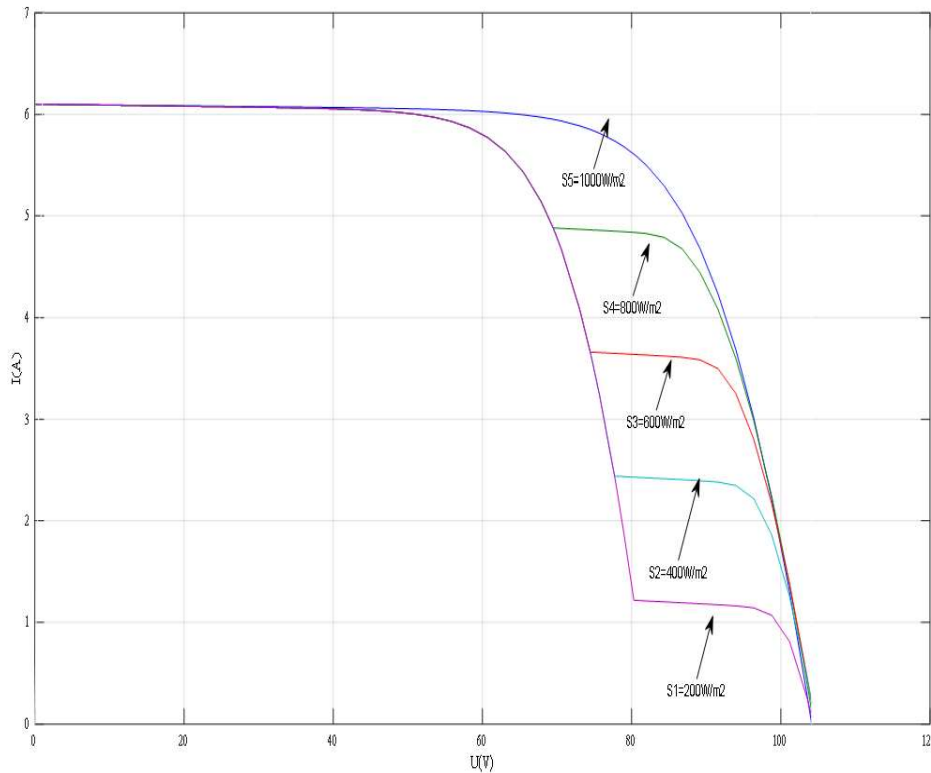


Fig.22 Partial shading conditions under different current variation with irradiated area

It is observed that when the irradiated area of a photovoltaic panel decreases, the total number of photons captured by the panel also decreases. This reduction in the number of photons received leads to a decrease in the current produced by the panel.

Adjusting the duty ratio is essential to maximize energy efficiency by regulating the energy extracted from the solar panel, ensuring that the system operates near its maximum power point (MPP) under varying sunlight conditions. Pulse Width Modulation is used for controlling the voltage of the converters, as shown in Fig. 23.

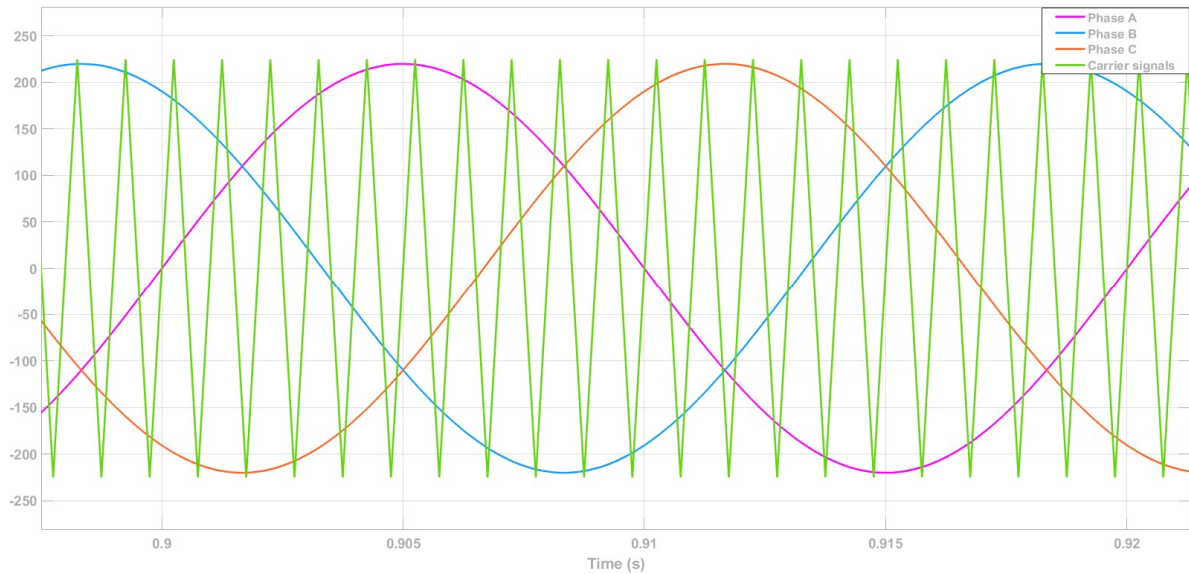


Fig.23 Sine Pulse width modulation

It is observed that Additionally, by using a sinusoidal reference, the inverter can operate more smoothly and efficiently, which is essential for maximizing the energy yield of solar panels and ensuring the stability of the power system. Adjusting the modulation index allows for precise control of the output voltage, which is especially useful under varying sunlight and temperature conditions.

This reduction in the number of photons received leads to a decrease in the current produced by the panel. As shown in Fig. 24 shows the variation of the duty cycle. Is also a technique used in inverters to generate an output of AC voltage from an input of DC with the help of switching circuits to reproduce a sinewave by generating one or more square pulses of voltages per half cycle.

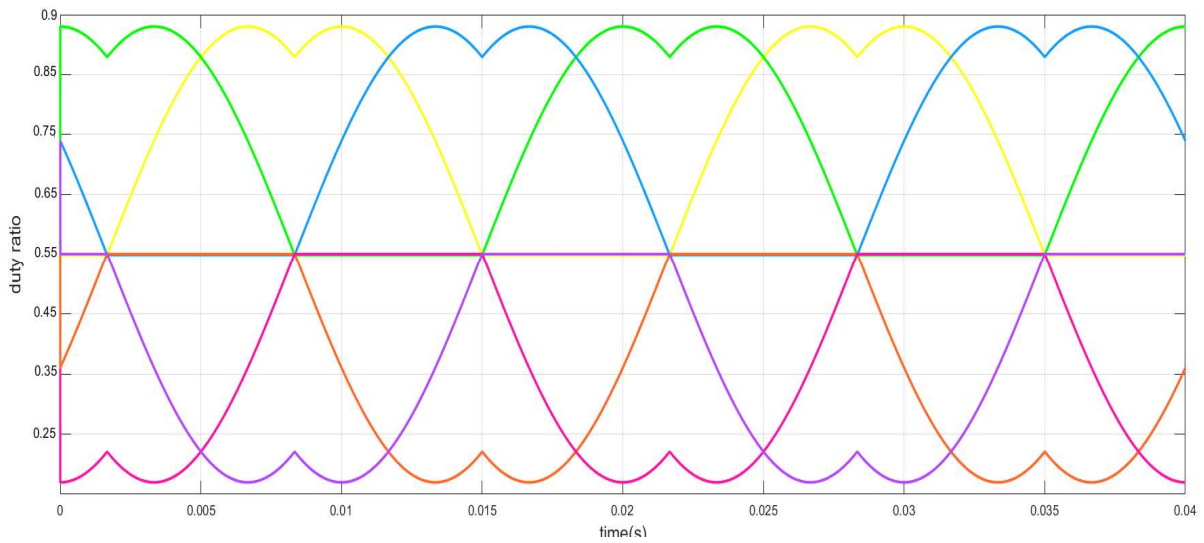


Fig.24 Sine Pulse width modulation

The duty cycle determines the duration of the switch is on, thus influencing the voltage and current of the PV system.

It is observed that the MPPT of RBFNN method by comparing, the results indicate a significant increase in accuracy, the experiment shows a strong correlation as follows in Fig. 26 and Fig. 27. In this study, a novel approach was developed to improve accuracy for training data-actual predicted and testing data actual predicted. The data were analyzed to determine the correlation, as shown in Fig. 26 and Fig. 27.

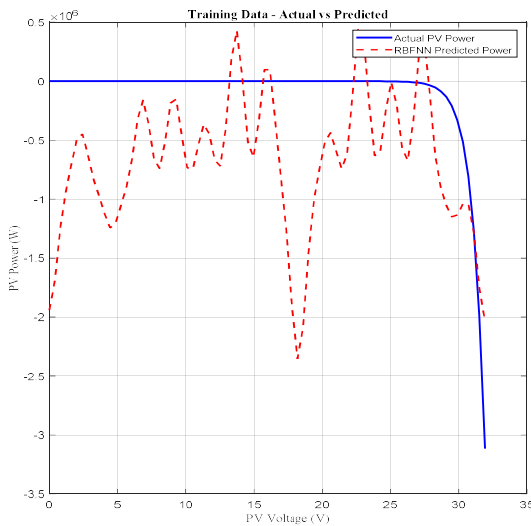


Fig.26 Training data actual and RBFNN predicted power under different voltage variation

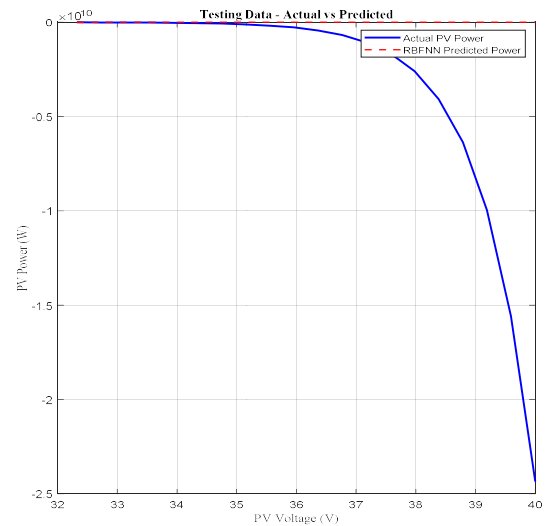


Fig.27 Testing data actual and RBFNN predicted power under different voltage variation

It is observed that, in this study a novel approach was developed to improve accuracy on solar photovoltaic fault diagnosis, the results indicate a significant increase in accuracy, a new strategy is being developed, the analysis of the data reveals significant trends, the experiment shows a strong correlation, as shown in Fig. 28.

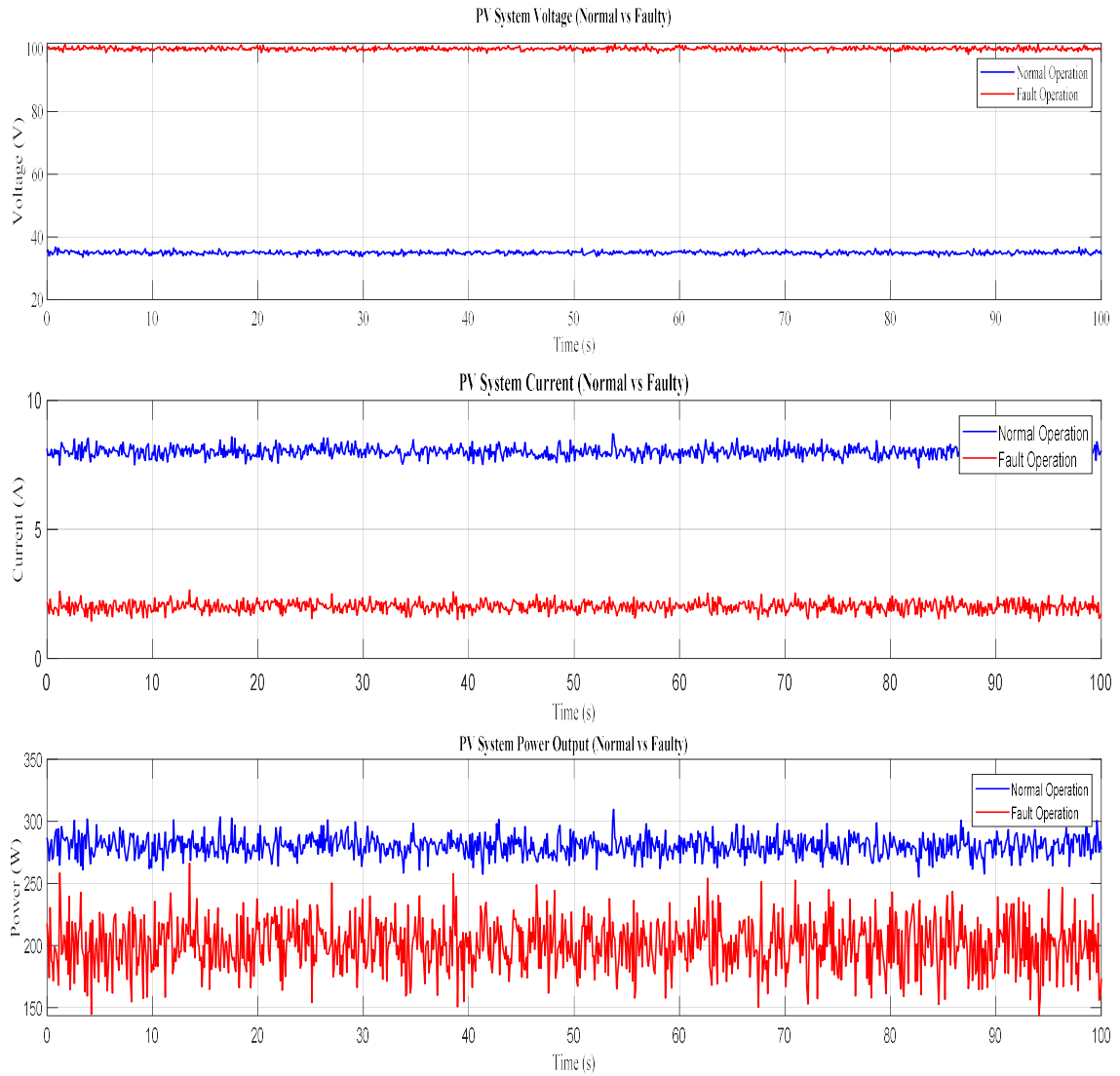


Fig. 28 Solar photovoltaic fault diagnosis on MPPT of RBFNN normal operation and Fault operation power, current and voltage variation

It is observed that, in this study a novel approach was developed to improve accuracy of the power, current and voltage on solar photovoltaic fault diagnosis, the analysis of the data reveals significant trends, a new strategy is being developed, the analysis of the data reveals significant trends, the experiment shows a strong correlation, as shown in Fig. 28.

Whereas a novel approach was developed to improve accuracy for RBFNN based on MPPT vs Conventional MPPT predicted as shown in Fig. 29.

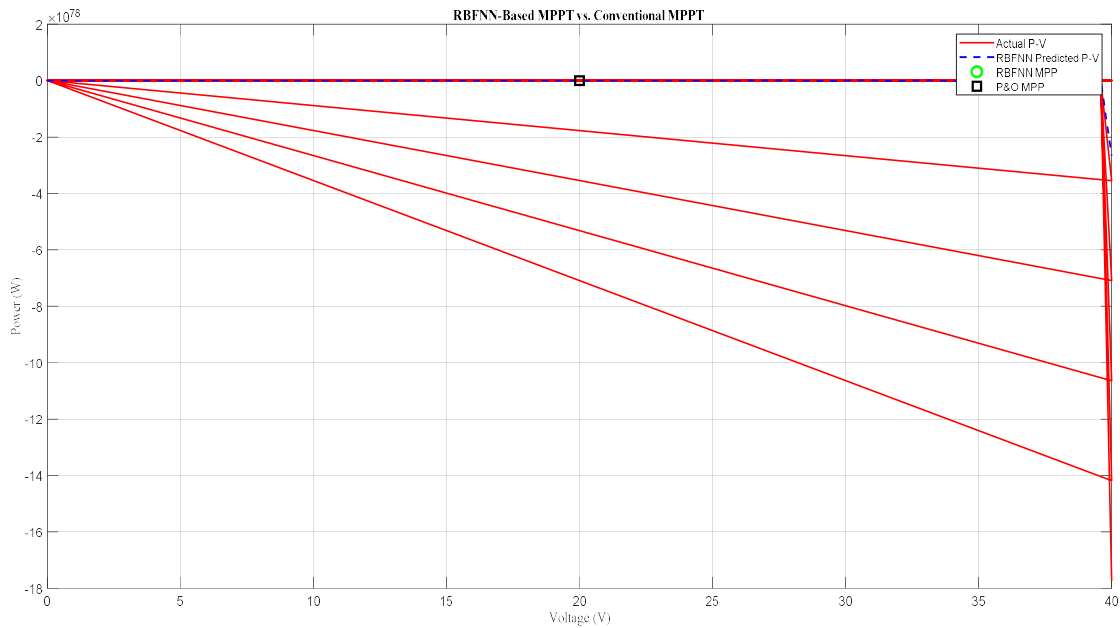


Fig.29 Solar photovoltaic fault diagnosis on RBFNN based on MPPT vs Conventional MPPT predicted operation and Fault operation on power and voltage variation

It is observed that, in this study a novel approach was developed to improve accuracy on RBFNN based on MPPT vs Conventional MPPT predicted on solar photovoltaic fault diagnosis, a new strategy is being developed, the analysis of the data reveals significant trends, the experiment shows a strong correlation, as shown in Fig. 29.

It is observed that, in this study a novel approach was developed to improve accuracy on solar photovoltaic fault diagnosis, a comparison of PV tracking the results indicate a significant increase in accuracy, a control strategy is being developed, the analysis of the data reveals significant trends, as shown in Fig. 30.

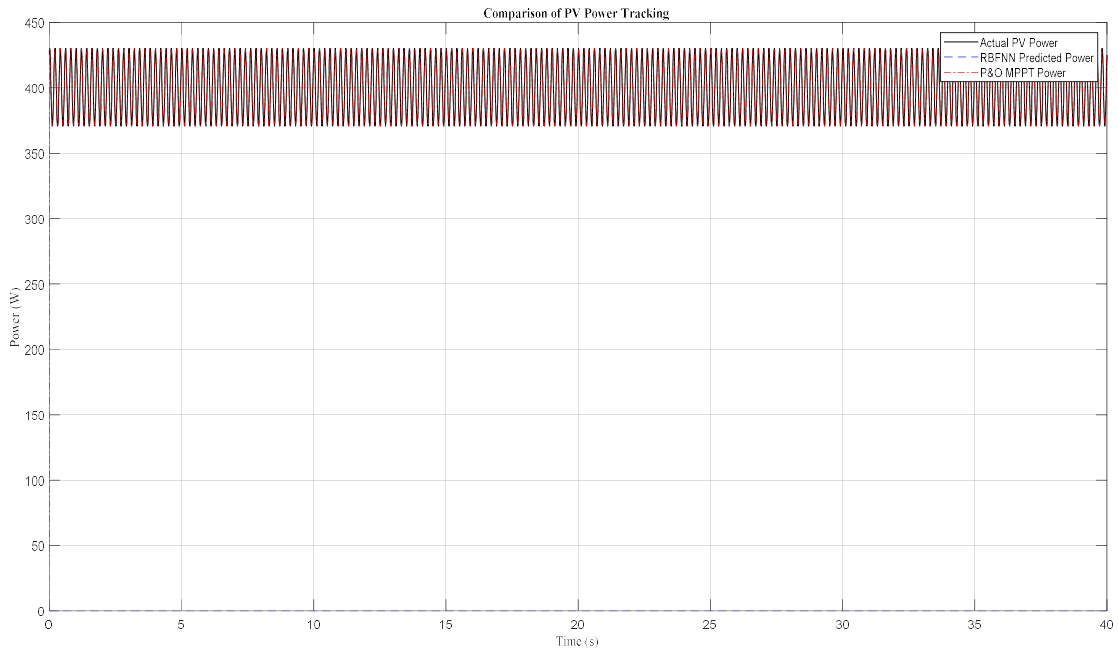


Fig. 30 Comparison of PV on Maximum Power Point Tracking and RBFNN Predicted Power

It is observed that, in this study a novel approach was developed to improve accuracy on solar photovoltaic fault diagnosis, a comparison of PV tracking the results indicate a significant increase in accuracy, a control strategy is being developed, the experiment shows a strong correlation, as shown in Fig. 30

It is observed that, in this study a novel approach was developed to improve accuracy on solar photovoltaic fault diagnosis, a radial basis functional neural network prediction of mean square error based on data collection: simulate or measure PV data under varying conditions, a significant increase in accuracy of the performance of data which is a system diagnosis of chaotic analysis neural network, a control strategy is being developed, the analysis of the data reveals significant trends, as shown in Fig. 31.

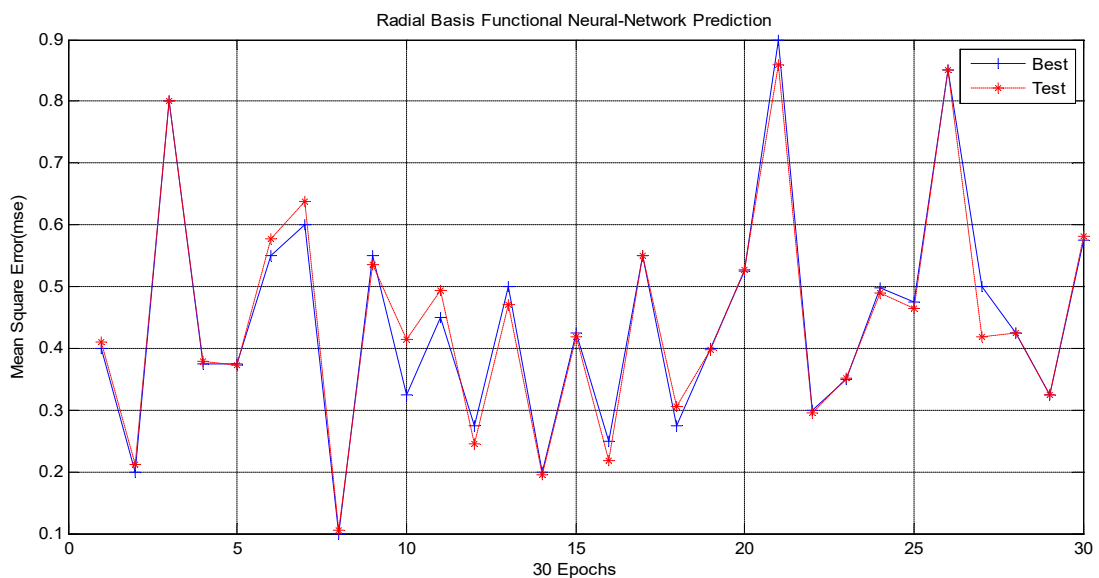


Fig. 31 System Diagnosis of Chaotic Analysis neural network

It is observed that, in this study a novel approach was developed to improve accuracy on solar photovoltaic fault diagnosis, a performance of data which is a system diagnosis of chaotic analysis neural network, the results indicate a significant increase in accuracy, a control strategy is being developed, the experiment shows a strong correlation, as shown in Fig. 31.

It is observed that, in this study a novel approach was developed to improve accuracy on solar photovoltaic fault diagnosis, a radial basis functional neural network of training, testing and validation, a significant increase in accuracy of the performance of data which is a system diagnosis of chaotic analysis neural network, a new strategy is being developed, the analysis of the data reveals significant trends, as shown in Fig. 32.

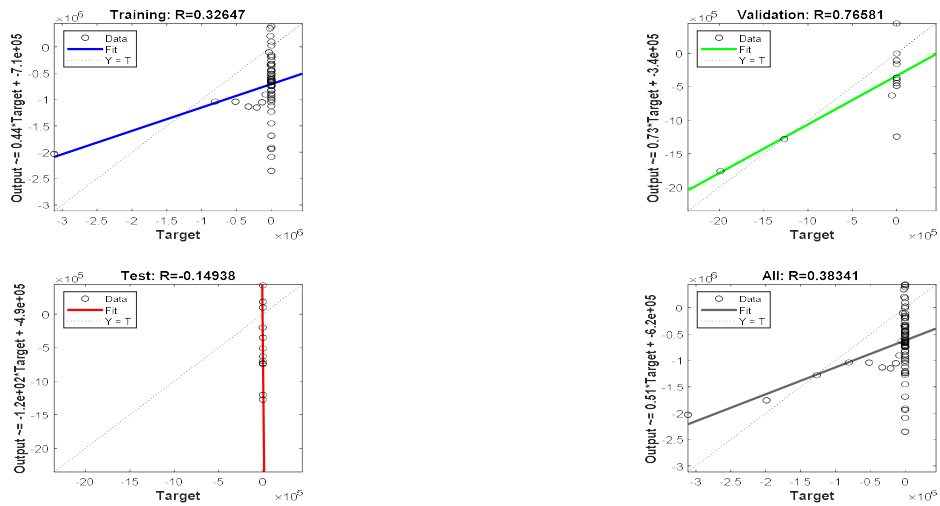


Fig. 32 Training and Testing of RBFNN System on PV and fault diagnosis

It is observed that, in this study a novel approach was developed to improve accuracy on solar photovoltaic fault diagnosis, a performance of data collection simulates or measures PV data under varying conditions, a control strategy is being developed, the experiment shows a strong correlation, Training and Test as shown in Fig. 32.

It is observed that, in this study a novel approach was developed to improve accuracy training and testing of best validation performance on solar photovoltaic fault diagnosis, a radial basis functional neural network, a significant increase as shown in Fig. 33.

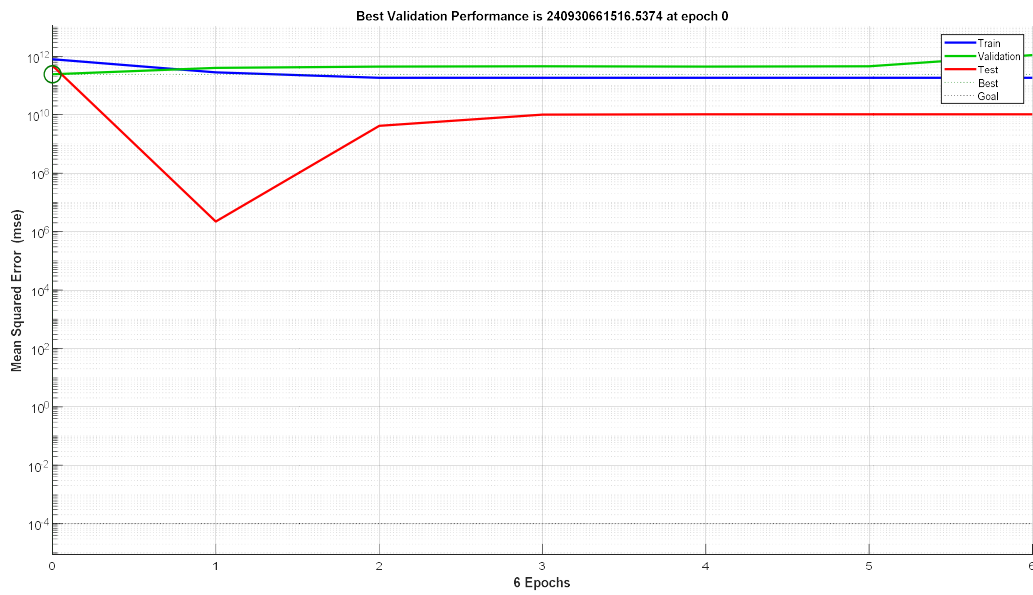


Fig. 33 A performance of mean square error a comparison of data collection,

It is observed that, in this study a novel approach was developed to improve accuracy on solar photovoltaic fault diagnosis, a performance of mean square error comparison of data collection, a control strategy is being developed, the experiment shows a strong correlation, the analysis of the data reveals significant trends, as shown in Fig. 33

Whereas in Fig. 34 shows the MPPT conventional based on Photovoltaic system, it is observed that, in this study a novel approach was developed to improve accuracy on solar photovoltaic to track that MPP.

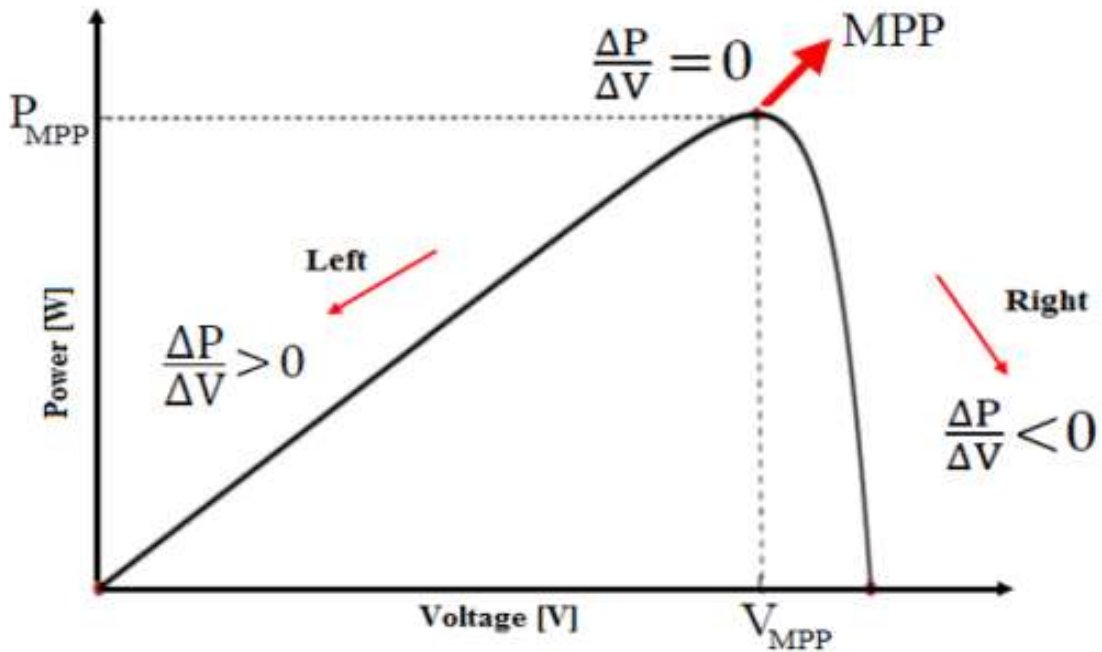


Fig.34. MPPT Algorithm

Where as an example shows, the scope $\frac{\Delta P}{\Delta U}$ can be calculated using the PV module voltage and current based on P&O algorithm. The incremental conductance algorithm is derived by differentiating the PV module power with respect to voltage and setting the results equal to zero. For a direct control scheme which directly controls the converter switching without external control loops, the considered step is the change in converter duty ratio ΔD as shown in Eqs. (61,62,63,64).

$$\Delta D = N_1 \frac{\Delta P}{\Delta U} \quad (61)$$

$$\Delta P = P(k) - P(k-1) \quad (62)$$

$$\Delta U = U(k) - U(k-1) \quad (63)$$

$$\Delta D = D(k) - D(k-1) \quad (64)$$

And N_1 is the scaling factor tuned at the design stage to adjust the conventional step-size ΔD to compromise between tracking accuracy as in [10,18] and its convergence speed.

Whereas the proposed of method of thr perturbation and observation is shown in Fig. 35 and also the proposed of method of the incremental conductance method is shown in Fig 36. The main advantage of using the incremental conductance method as in (e.g. [10],[11]) is that the control strategy, robust and optimal stability of the MPPT is high.

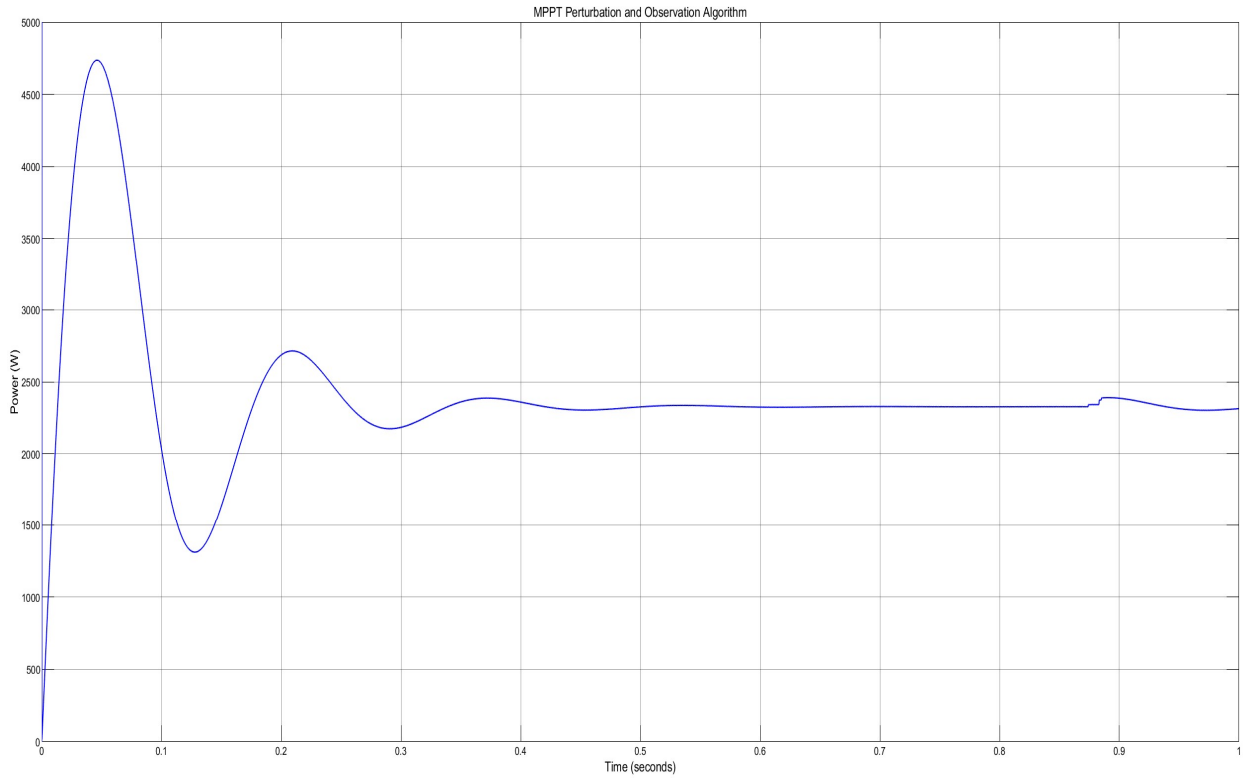


Fig. 35 MPPT Perturbation and Observation Algorithm

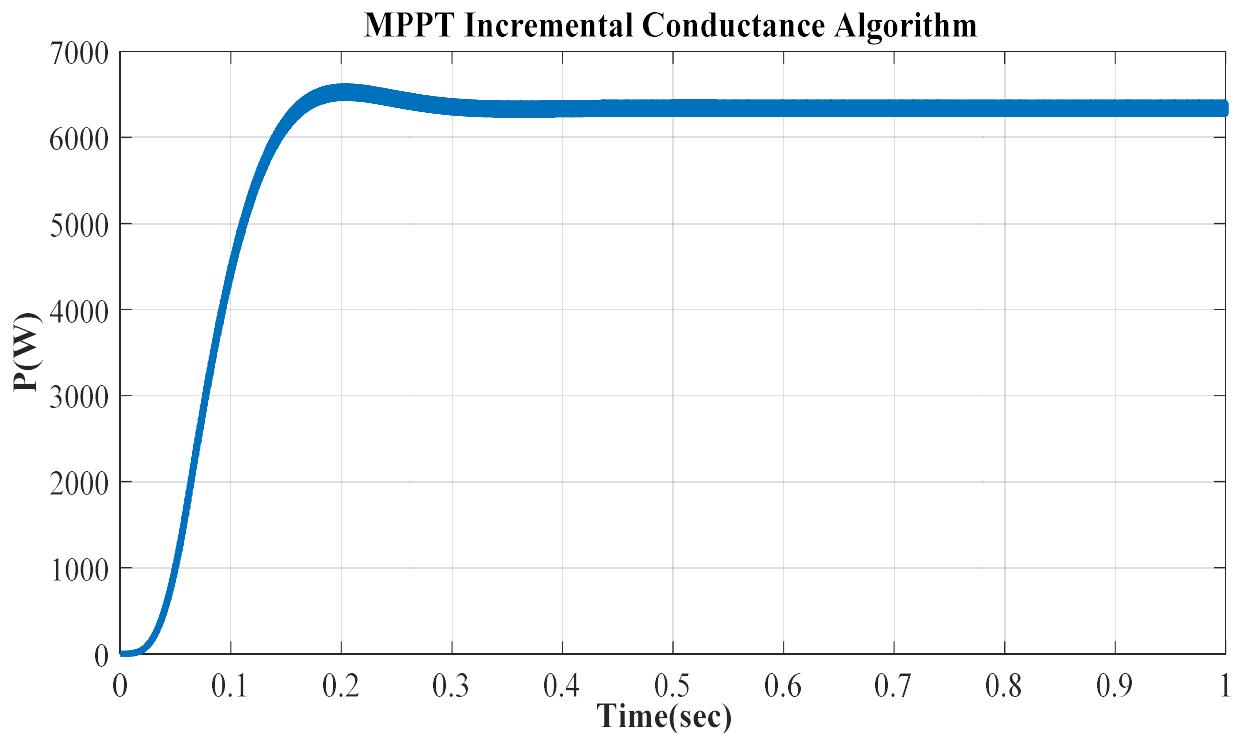


Fig. 36 MPPT Incremental Conductance Algorithm

Whereas the neural network shows of multiple layers of neurons; the input end is called input layer and the output end is called output layer. The hidden layer is between the output layer and input layer as shown in Fig. 37

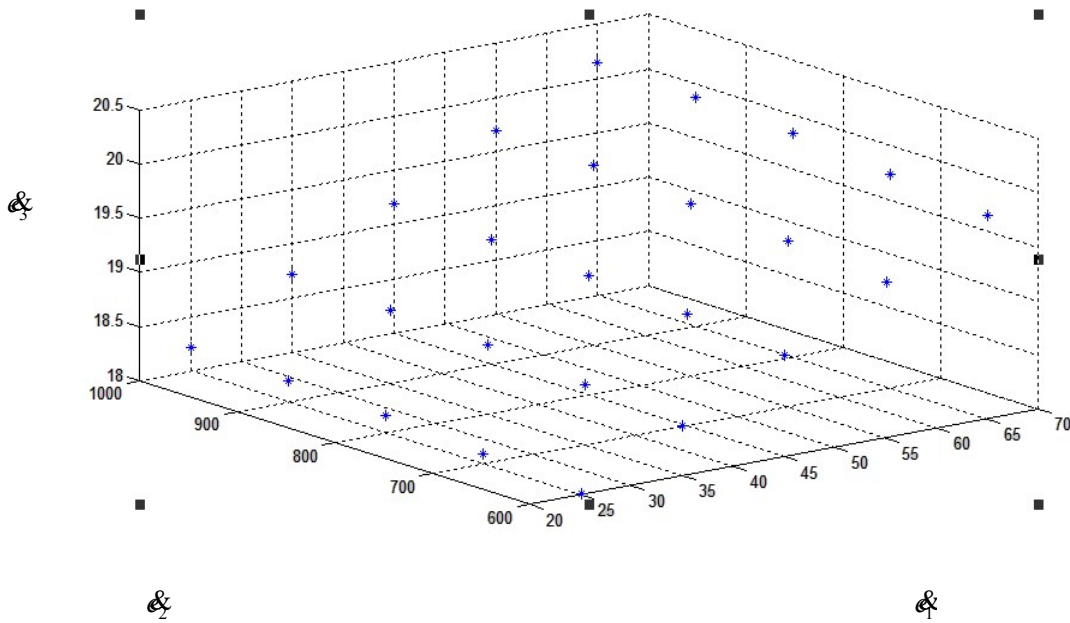


Fig. 37 Three-dimensional diagram of normal chaotic dynamic error at 1000W/m²

Performance evaluation techniques are discussed on the basis of the dynamic parameters of the PV system although the control of this structure is relatively advanced technology but the conversion efficiency is difficult to improve due to increase in transformation series. The range of extension field was determined by neural network numerical simulations are implemented for illustration and verification of the effectiveness of radial basis function neural network control strategy which are MPPT algorithm and inverter control to the electrical grid of Republic of Congo and their influences on the dynamic performance of the system and their impact in reducing the harmonic rate for better injection into the grid, compared the diagnostic rates with the results by others. Whereas these harmonics can be reduced by filters to improve the quality of the AC waveform and, consequently, the active power as shown in Fig. 38 illustrates the harmonic distortion rate.

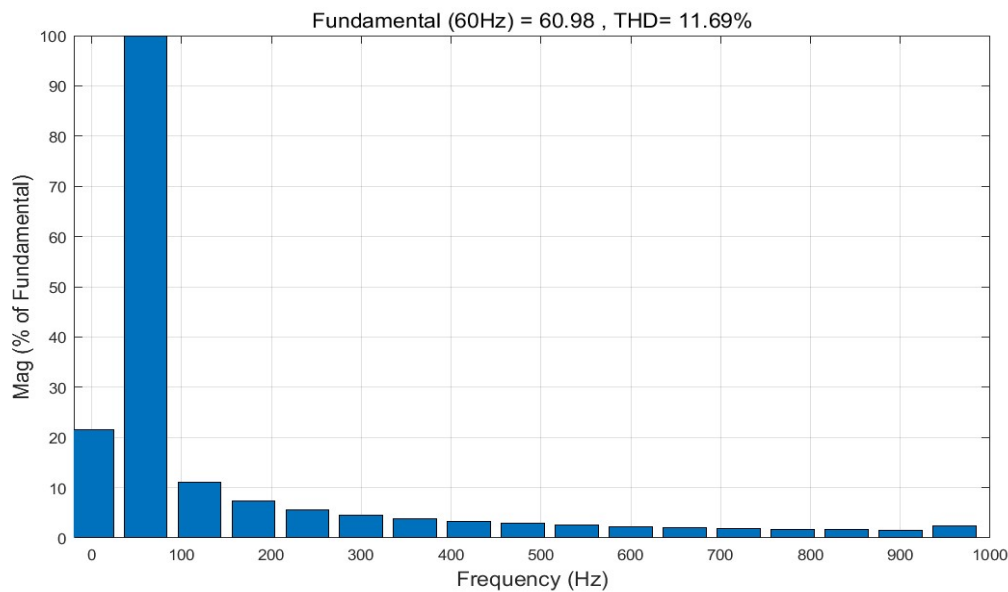


Fig. 38 Harmonic distortion rate.

IV. CONCLUSIONS

A case study has been conducted to highlight certain performance issues of MPPT (Maximum Power Point Tracking) Algorithm. This study presented a representative model of a three-phase photovoltaic system connected to the electrical of the grid-connected of the Republic of Congo, aiming to diagnostic the MPPT. We applied the Radial Basis Function Neural Network (RBFNN) method, by comparing while Perturbation & Observation and Incremental Conductance compares the attributes of various conventional, significance and novelty of proposed on control strategy, the RBFNN system is integrated into the control scheme of the grid – connected PV system. The range of extension chaotic field of diagnosis was determined by Radial Basis Function Neural Network numerical simulations are implemented for illustration and verification of the effectiveness of Radial Basis Function Neural Network control strategy which are MPPT Algorithm, tracks the maximum power point using RBFNN the input variables, Irradiance and Temperature are mapped to an optimal duty cycle and inverter control for a three –phase signal grid connected inverter based on real time gird conditions Voltage and frequency synchronization. A model of three single-phase PV grid-connected system is built, and simulation results show the RBFNN MPPT algorithm has excellent dynamic and static performances, which verifies fault diagnosis method is effective for RBFNN MPPT Algorithm in the single-stage and three single-phase PV grid-connected system.

A robust and optimal control system of the proposed of method have improved on incremental conductance algorithms, perturbation and observation control techniques, and other maximum power point tracking (MPPT) algorithms in normal and partial shading conditions and observed an improvement in the performance of the grid-connected photovoltaic system.

To minimize potential perturbation errors of the RBFNN algorithm because of the improved of the incremental conductance algorithm due to rapid irradiation changes also better than P&O algorithm low cost, the fundamental harmonic frequencies are in the range of 0 to 100 Hz, with a total harmonic distortion rate of 11.69%. Although this harmonic distortion rate has seen high, this paper proposes an enhanced MPPT with

chaos extension radial basis function neural network of Maximum Power Point Tracking (MPPT) algorithms based on fault diagnosis method in single-stage three-phase photovoltaic (PV) systems connected to the grid of Congo-Brazzaville by others. The steady –state and dynamic responses are illustrated according to the chaos extension radial basis function neural network of Maximum Power Point Tracking (MPPT) algorithms and advanced circuit structure and appropriate control strategy PV Grid connected with the high cost and low efficiency, we have investigated the enhanced MPPT with chaos extension radial basis function neural network of Maximum Power Point Tracking (MPPT) algorithms based on fault diagnosis method in single-stage three-phase photovoltaic (PV) systems connected to the grid of Congo-Brazzaville. In the future we will consider the adaptive of RBFNN on fault diagnosis method in single-stage three-phase photovoltaic (PV) systems connected to the grid of Congo-Brazzaville

ACKNOWLEDGMENT

This work was supported by Key Research and Development Program in the Republic of Congo-Brazzaville of funding and with affiliated of Chinese Laboratory.

REFERENCES

- [1] M. Rowen, M. Jamil, and D. P. Kothari, “Generalized Neural Network approach for global solar energy estimation in India,” *IEEE Transactions on Sustainable Energy*, vol. 3, no. 3, pp. 576–584, 2012.
- [2] H. A. Table and K. Khorasani, “A neural network-based Multiplicative actuator fault detection and isolation of nonlinear Systems,” *IEEE Transactions on Control Systems Technology*, vol.21, no. 3, pp. 842–851, 2013.
- [3] S. Yousef and A. K. Mahmood, “Fault diagnosis in internal Combustion engines using extension neural network,” *IEEE Transactions on Industrial Electronics*, vol. 61, no. 3, pp. 1434–1443, 2014.
- [4] Y. Wu, Q. Lan, and Y. Sun, “Application of BP neural network Fault diagnosis in solar photovoltaic system,” in *Proceedings of the IEEE International Conference on Mechatronics and Automation (ICMA '09)*, pp. 2581–2585, Changchun, China, August 2009.
- [5] S. Syafaruddin, E. Karatepe, and T. Hiyama, “Controlling of Artificial neural network for fault diagnosis of photovoltaic array,” in *Proceedings of the 16 th International Conference on Intelligent System Applications to Power Systems (ISAP '11)*, Hersonissos, Greece, September 2011.
- [6] T. Shimakage, K. Nishioka, H. Yamane, M. Nagura, and M. Kudo, “Development of fault detection system in PV system,” in *Proceedings of the IEEE 33rd International Telecommunications Energy Conference (INTELEC '11)*, pp. 1–5, Amsterdam, The Netherlands, October 2011.
- [7] Y. Zhao, L. Yang, B. Lehman, J.-F. de Palma, J. Mosesian, and R. Lyons, “Decision tree-based fault detection and classification in solar photovoltaic arrays,” in *Proceedings of the 27th Annual IEEE Applied Power Electronics Conference and Exposition (APEC '12)*, pp. 93–99, Orlando, Fla, USA, February 2012.
- [8] M. Tadj, K. Benmouiza, A. Cheknane, and S. Silvestre, “Improving the performance of PV systems by faults detection using GISTEL approach,” *Energy Conversion and Management*, vol.80, pp. 298–304, 2014.

- [9] C.-T. Hsieh, H.-T. Yau, and J. Shiu, “Chaos synchronization Based novel real-time intelligent fault diagnosis for photovoltaic Systems,” *International Journal of Photo energy*, vol. 2014, Article ID759819,9 pages, 2014.
- [10] Tey, K.S.; Mekhilef, S. Modified incremental conductance MPPT algorithm to mitigate inaccurate responses under fast-changing solar irradiation level. *Sol.Energy* 2014,101,333-342 [CrossRef]
- [11] Sivakumar, P.; Kader, A.A; Kaliavaradhan, Y.; Arutchelvi, M. Analysis and enhancement of PV efficiency with incremental conductance MPPT technique under nonlinear loading conditions. *Renew.Energy* 2015,81 543-530 [CrossRef]
- [12] K.-H. Chao, S.-H. Ho, and M.-H. Wang, “Modeling and fault Diagnosis of a photovoltaic system,” *Electric Power Systems Research*, vol. 78, no. 1, pp. 97–105, 2008.
- [13] Babu, T.S.; Rajasekar, N.; Sangeetha, K. Modified particles optimization technique based maximum power point tracking for uniform and under partial shading conditions. *Appl.Soft Comput.*2015, 34,613-624.
- [14] Kotti, R.; Shireen, Efficient MPPT control for PV systems adaptive to fast changing irradiation and partial shading conditions. *Sol. Energy* 2015 114, 397-407.
- [15] Harrag, A.; Messalti, S. Variable step size modified P&O MPPT algorithm using GA-based hybrid offline/online PID controller. *Renew. Sustain. Energy Rev.* 2015, 49,907-920 [CrossRef]
- [16] Verma, D., Neme, S.; Shandilya, A.; Dash, S.K. Maximum power tracking (MPPT)techniques: Recapitulation in solar photovoltaic system. *Renew. Sustain. Energy Rev.*2016, 54,1018-1034. [CrossRef]
- [17] Li, X.; When, H.; Jiang, L., Xiao, W.; Du, Y.; Zhao, C. An improved MPPT Method for System with Fast-Converging Speed and Zero Oscillation. *IEEE Trans.Ind.Appl.*2016, ,5051-5064 [CrossRef]
- [18] Ling, L.; Wu, X.; Liu, M.; Zhu, Z.; Li ,Y.; Shang, Development of photovoltaic hybrid LED street lighting system. In Proceedings if the 2016 IEEE Advanced Information Management, Communicates, Electronic and Automation Control Conference (IMCEC), Xi’ an, China, 3-5Octobre 2016; pp.729-732.
- [19] Loukriz, A.; Haddadi, M.; Messalti, Simulation and experimental design of a new advanced variable step size Incremental Conductance MPPT algorithm for PV systems *ISA Trans.*2016,62,30-38.
- [20] Husain, MA; Tariq, A.; Hameed, S; Arif, M S B; Jain, A. Comparative assessment if maximum power point tracking procedures for photovoltaic systems. *Green Energy Environ.* 2017, 2, 5-17[CrossRef].
- [21] Dousoky, G.M.; Shoyama, M. New parameter for current-sensor less, MPPT in grid-connected photovoltaic VSIs.*Sol. Energy* 2017,143,11, -119. [CrossRef].
- [22] Messalti, S.; Harrag, A.; Loukriz, A. A new variable step size neural networks MPPT controller: Review, simulation and hardware implementation. *Renew. Sustain. Energy Rev.* 2017, 68,221-233. [CrossRef]
- [23] Ezinwanne, O.; Zhongwen, F.; Zjijun, L.; Energy Performance and Cost Comparison of MPPTtechniques for Photovoltaics and other Applications *Energy procedia* 2017,107,297-303[CrossRef].
- [24] Tey, K.S.; Mekhilef, S.; Seyedmahmoudian, M.M; Horan, B.: Oo, A.M.T.; Stojcevski, A. Improved Differential Evolution –based MPPT Algorithm using SEPIC for PV system under Partial Shading Conditions and Load Variation. *IEEE Trans.Ind. Inform.*2018 [CrossRef].